JCAMECH

Vol. 50, No. 2, December 2019, pp 324-340
DOI: 10.22059/jcamech.2019.282149.401

Nonlinear analysis of radially functionally graded hyperelastic cylindrical shells with axially-varying thickness and non-uniform pressure loads based on perturbation theory

Hamed Gharooni[a] *and Mehdi Ghannad*[a,*]

[a] Department of Mechanical Engineering, Shahrood University of Technology, Shahrood, Iran

ARTICLE INFO

Article history:
Received
Received in revised form
Accepted
Available online

Keywords:
Hyperelastic FGMs
FG cylindrical shells
Variable thickness
Perturbation theory
Hyperelastic pressure vessel

ABSTRACT

In this study, nonlinear analysis for thick cylindrical pressure vessels with arbitrary variable thickness made of hyperelastic functionally graded material properties in nearly incompressible state and clamped boundary conditions under non-uniform pressure loading is presented. Thickness and pressure of the shell are considered in axial direction by arbitrary nonlinear profiles. The FG material properties of nearly incompressible hyperelastic shell are graded in the radial direction with a power law distribution. Effective combination of shear deformation theory and match asymptotic expansion of perturbation theory are used to derived and solve the nonlinear governing equations, respectively. A numerical modelling based on finite element method is presented to validate the results of the current analytical solution. The effect of material constants, non-homogeneity index, geometry and pressure profiles on displacements, stresses and hydrostatic pressure distributions are illustrated for different hyperelastic material properties and case studies. This approach enables insight to the nature of the deformation and stress distribution through the thickness of rubber vessels and may offer the potential to study the mechanical functionality of blood vessels such as artificial or natural arteries in physiological pressure range

1. Introduction

Thick hyperelastic shells in the presence of large displacements and strains with nonlinear elastic constitutive laws are typically used for the modeling of rubber-like materials and biological tissues. In such cases, a fully nonlinear formulation, including both kinematic and constitutive nonlinearities, needs to be adopted. The incompressible or nearly-incompressible hyperelasticity, including geometrical and material nonlinearities, is the ability of a material to incident large elastic strain due to small forces, without losing its original properties. Rubber-like hyperelastic materials are usually modeled as incompressible or nearly incompressible nonlinear elastic. These materials are often used to make tires, catheters, water hoses, shock absorbers, fenders for boats, seals, cylindrical sleeves in label printing and packer rubbers. The mathematical modelling of the mechanical behaviour of rubber-like hyperelastic materials focuses to a large extent on the development of an appropriate form of a strain energy function applicable to the range of deformations of interest to practical applications. Common practical constitutive relations for studying the mechanical deformations of these materials include the neo-Hookean and the Mooney-Rivlin. The neo-Hookean model provides a good description of the mechanical properties of rubber materials when deformation is less than 70%. A comprehensive survey on the finite element methods of incompressible or almost incompressible hyperelastic materials can be found in many papers [1]. As an important primary research, Sussman and Bathe [2] introduce a displacement-pressure finite element formulation for the geometrically and materially nonlinear analysis of compressible and almost incompressible solids. Doll and Schweizerhof [3] developed the volumetric part of the strain energy function and investigated new volumetric functions. Lopez-Pamies [4] proposed a new I1 based hyperelastic model, much like the neo-Hookean one, for rubber elastic solids applicable over the entire range of deformations. Bijelonja et al. [5] presented development of a displacement-pressure based finite volume formulation for modelling of large strain problems including incompressible hyperelastic materials with a Mooney–Rivlin model. The problem of the finite axisymmetric deformation of a thick-walled circular cylindrical elastic tube subjected to pressure is formulated for an incompressible isotropic neo-Hookean material by Zhu et al. [6] and solved numerically by finite element library Libmesh. Tanveer and Zu [7] presented finite amplitude transient vibration analysis of nearly incompressible hyperelastic axisymmetric solids by a mixed p-type method and solved the equations by the Newmark's method along with the Newton–Raphson iterative technique for hyperelastic material description. Montella et al. [8] presented the mechanical behavior of a Tire Derived Material (TDM) in details numerically and experimentally. They fitted some hyperelastic models to the collected experimental data to investigate the rate-independent behavior of these materials as

* Corresponding author. Tel.: +98-23-32300240-3340; fax: +98-23-32300258; e-mail: Ghannad.mehdi@gmail.com

anti-vibration in railway track applications. Kiendl et al. [9] presented formulations for compressible and incompressible hyperelastic thin shells with plane stress condition based on energy methods and used continuous iso-geometric discretization to build the numerical solution.

Since the early studies of hyperelastic theories related to rubber-like materials, their range of applications have been extended to include biological materials and synthetic soft tissues used in bio-medical engineering. Investigating aortic aneurysm as pressurized hyperelastic blood vessels enable scientists to evaluate the relative sensitivity of displacement and stress to geometrical and mechanical properties of the aneurysmal tissue. Furthermore, in pathologic conditions, arteries are even under more shear deformation compared to healthy vessels [10]. In clinical interventions, such as balloon angioplasty significant wall shearing may take place. Simulation of arteries under blood pressure to yield displacement and stress analysis of blood vessels could result in useful information on the behavior of the arterial tissues under shear deformation [11]. Mihai and Goriely [12] investigated universal relations between parameters of different hyperelastic material models which are used to quantify nonlinear elastic responses of several hyperelastic models as rubber structures to soft tissues. Utilizing a computational approach, Scotti et al. [13] studied the effects of geometry asymmetry and wall thickness, two vital parameters that intensify risk of aneurysm rupture, on deformation and stress of virtual abdominal aortic aneurysm (AAA). Lally et al. [14] investigated the effect of different stent designs on level of deformation and stress in the vascular wall of stented arteries based on FEM for developing novel stent designs. A review of some specific and pioneer constitutive models proposed for hyperelastic energy densities of soft biological tissues were presented in literature [15].

Depending upon the intended applications, material properties of rubber-like material models may be desirable to vary in one or more directions for optimizing the life of structures. This purpose can be achieved by either changing the chemical composition or fabricating the component from two or more materials [16]. Graded rubber-like materials attracted the attention of researchers for modeling these materials behavior under mechanical and geometrical boundary conditions. For instance, effects of material inhomogeneities on stress distributions through the thickness of circular cylinders made of rubber-like materials in mechanical and thermal load was studied by Bilgili [17]. In another study, Bilgili [18] investigated plane strain deformations of a circular cylinder made of heterogeneous neo-Hookean material with circumferential displacements prescribed on the inner and the outer surfaces. Lopez-Pamies and Castaneda [19] have used a second-order homogenization method to determine the overall constitutive response of an elastomer reinforced with either rigid or compliant fibers and subjected to finite deformations. Batra and Bahrami [20] considered cylindrical pressure vessel made of FG rubber-like material under internal pressure. To discover stress components of the pressure vessel, they assumed axisymmetric radial deformations of a circular cylinder composed of FG Mooney–Rivlin material with the material parameters varying continuously through the radial direction by a power law relation. Anani and Rahimi [21, 22] studied behavior of spherical and cylindrical shell made of FG rubbers by neo-Hookean model. They assumed radial variation of material properties by power law function and used classical theory (PET) and Gauss-hypergeometric function to derive and solve equations, respectively. Geometrically nonlinear dynamic behavior of FG thick hollow cylinder under axisymmetric mechanical shock loading is investigated by Ghadiri Rad et al. [23]. They used meshless local Petrov–Galerkin method to analyze cylinder made of neo-Hookean materials such as carbon-based polymers.

In optimizing FG structures with respect to weight or stress distribution, one method is to use shells with varying thickness or materials properties along one or two direction. The literature that addresses the stresses of thick cylindrical shells with variable thickness is quite limited. Eipakchi [24] calculated stresses and displacements of linear elastic conical shell with varying thickness under non-uniform internal pressure analytically, using shear deformation theory (SDT). Gharooni and Ghannad [25] investigated thermo-elastic analysis in pressurized thick FGM cylinders with varying properties of power function based on higher-order shear deformation theory. The innovative formulations for higher-order approximation with FG function of materials properties have been presented in this research. Ghannad et al. [26] presented a closed-form analytical solution for thick FGM cylindrical shells with variable thickness subjected to constant internal pressure based on the first-order shear deformation theory (FSDT) and solved the governing equations by the usage of perturbation theory. Jabbari et al. [27] investigated thermo-elastic analysis of rotating truncated conical shells with varying thickness made of functionally graded materials (FGMs) subjected to thermo-mechanical loading. The system of partial differential equations is semi-analytically solved by using multi-layered method (MLM). Nejad et al. [28] presented semi-analytical solution for elastic analysis of axially functionally graded rotating thick cylindrical shells with variable thickness under non-uniform pressure by the usage of SDT and MLM. Mazarei et al. [29] presented an exact closed-form analytical solution to solve the thermo-elasto-plastic problem of thick-walled spherical vessels made of functionally graded materials. Material properties were graded in the thickness direction according to a power law distribution and the plastic model was based on von Mises yield criterion and its associated flow rules under the assumption of perfectly plastic material behavior. Nejad et al. [30] investigated exact solutions for purely elastic, partially plastic and fully plastic deformation and stresses of rotating FG cylindrical pressure vessels with radial variations of material properties under thermal load. Stress distribution in a functionally graded nanodisk of variable thickness under thermal and mechanical loads and constant angular velocity was obtained by Hosseini et al. [31] based on the strain gradient theory and numerical scheme. Mechanical properties of the nanodisk were assumed to vary according to the power law formulation in radial direction. However, there are practical occasions which require tailored grading of properties in two directions, the number of studies on structures made of two-directional functionality is very limited. As important researches, Nejad and Hadi [32] applied Eringen's non-local theory to investigate size effects on vibration analysis of Euler–Bernoulli nano-beams made of bi-directional functionally graded material in both axial and thickness directions of the beam. Buckling analysis of the nano-beams made of two-directional functionally graded materials with small scale effects was carried out by Nejad et al. [33] based on the nonlocal elasticity theory. They presented a solution by the usage of generalized differential quadrature method and taking into account the variation of FG material properties with arbitrary functions along thickness and length direction. Nejad et al. [34] investigated the bending of Euler-Bernouilli nano-beams made of bi-directional functionally graded materials using Eringen\'s non-local elasticity theory and the Rayleigh-Ritz method. Bi-directional functionality, similar to the previous article, was assumed for FGMs nano-beam.

Although numerous studies have been carried out on compressible or nearly incompressible hyperelastic shells, no

analytical analysis has been carried out to date on non-uniformly pressurized cylinder with nonlinear variable thickness made of hyperelastic FGMs. On the other hand, most of the mentioned numerical methods are not efficient for incompressible materials. The common problems with these studies, as Poisson's ratio approaches 0.5, are the ill conditioning of stiffness matrix, the locking phenomena and effect of applying numerical techniques on resulted displacements and stresses. Using multi-layered method, linear elastic semi-analytical solution of axially functionally graded thick cylindrical shells with variable thickness could be demonstrated. However, one could divide the length of the cylinder into several disks with uniform material properties in each layer and analyze a multi-body problem with tractions and displacement continuity conditions imposed at interfaces between adjoining disks, this semi-analytical approach is not suitable in nonlinear modeling of FG hyperelastic variable thickness shells with radial variation of the material properties. Furthermore, no exact or analytical solution could be demonstrated for these geometrically and materially nonlinear complex problems based on plane or 3D elasticity theories. But analytical solutions have their own advantages; one can use these methods in optimizing shell thickness with trial and error, provided that displacements or stresses are considered as the objective functions, by preparing a mathematical program to analyze various models. They are more efficient respect to the FE modeling because the related programs can be run by a few variations and don't require constructing FE modeling and meshing.

In the current study, nonlinear quasi-static analysis of thick cylindrical pressure vessels with arbitrary variable thickness made of neo-Hookean model of hyperelastic FGM with radially-varying properties in nearly incompressible state under non-uniform pressure loading is presented. The thickness and pressure profiles of the vessel are considered as the arbitrary nonlinear function of axial direction. The nonlinear governing equations have been derived by using first-order shear deformation theory. Match Asymptotic Expansion (MAE) of the perturbation theory is used for solving the governing system of nonlinear coupled differential equations with variable coefficients. The article is proposing to solve a very complex case containing geometrically and materially nonlinear shells undergoing large displacements and strains and benchmarks for non-linear problems. A new ingenious formulation and parameters have been defined during current study to simplify and abbreviate the representation of inner and outer equations components in MAE. The effect of materials constants, inhomogeneity index, geometry and pressure profiles on displacements, stresses and hydrostatic pressure distributions resulting from MAE solution have been investigated for different hyperelastic material properties and case studies and the results have been compared with FE modeling in ANSYS software. We present the equations that provide the general continuum description of the deformation and the hyperelastic stress response of the material. Current study aims to illustrate the potentials and reliability for estimating the state of deformation and stress in hyperelastic FG vessels from rubber structures to arteries.

2. Basic formulations

2.1. Shear deformation theory

Fig. 1 show geometry, loading and boundary conditions of a thick-walled axisymmetric cylindrical shell with arbitrary variable thickness under non-uniform pressure loading in the reference configuration. The location of any typical point, within the shell element may be determined by radius of mid-plane $R(x)$ and distance of typical point from the middle surface z, as

$$r = R(x) + z \ , \ -\frac{h(x)}{2} \le z \le \frac{h(x)}{2}, \quad 0 \le x \le L \tag{1}$$

$h(x)$ and L are axially variable thickness and length of the shell, respectively. The following relations can be written for the geometry components of the shell:

$$R(x) = r_i + \frac{h(x)}{2}, \quad r_o(x) = r_i + h(x) \tag{2}$$

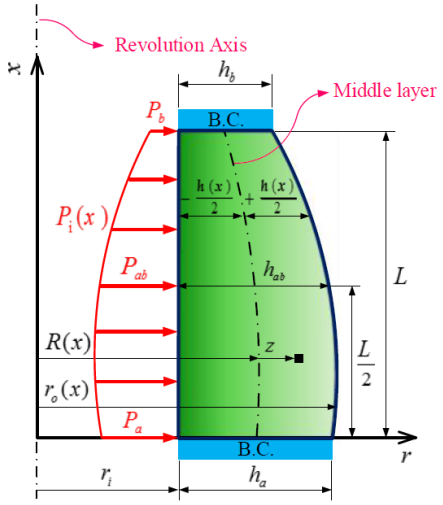

Figure 1. Geometry, loading and boundary conditions in cross section of the shell.

In the first-order shear deformation theory, the general axisymmetric displacement field can be expressed in the following form based on axial and radial displacement components.

$$U_z(z,x) = w(x) + z\psi(x), \quad U_x(z,x) = u(x) + z\varphi(x), \quad U_\theta = 0 \tag{3}$$

where $w(x)$ and $u(x)$ are the displacement components of the middle surface. Also, $\psi(x)$ and $\varphi(x)$ are the function of displacement field. In geometrically nonlinear kinematic, deformation gradient tensor $[\mathbf{F}]$ can be written based on displacements components as [6]

$$[\mathbf{F}] = \begin{bmatrix} 1+\psi & 0 & w' + \psi' z \\ 0 & 1 + \dfrac{w + \psi z}{R + z} & 0 \\ \varphi & 0 & 1 + u' + \varphi' z \end{bmatrix} \tag{4}$$

where $(\ )' = \partial(\ )/\partial x$. Considering the definition of right Cauchy–Green deformation tensor as $[\mathbf{C}] = [\mathbf{F}]^{\mathrm{T}}[\mathbf{F}]$, its principal invariants $I_{1,2,3}$ and the volume ratio of deformation (Jacobian) in cylindrical polar coordinate system can be written

$$\begin{cases} [\mathbf{C}] = \begin{bmatrix} C_{zz} & 0 & C_{zx} \\ 0 & C_{\theta\theta} & 0 \\ C_{xz} & 0 & C_{xx} \end{bmatrix}, & \begin{aligned} I_1 &= C_{zz} + C_{\theta\theta} + C_{xx} \\ I_2 &= C_{zz}C_{\theta\theta} + C_{\theta\theta}C_{xx} + C_{zz}C_{xx} - C_{zx}^2 \\ I_3 &= C_{zz}C_{\theta\theta}C_{xx} - C_{\theta\theta}C_{zx}^2 = J^2 \end{aligned} \\ J = \det(\mathbf{F}) = \left(\dfrac{1}{R(x)+z}\right)\Big[(R(x) + z + w + \psi z) \\ \qquad \big((1+\psi)(1+u'+\varphi' z) - \varphi(w' + \psi' z)\big)\Big] \end{cases} \tag{5}$$

'det' stands for determinant operator. The strain–displacement relations in matrix representation of Green–Lagrange strain tensor can be defined as $\mathbf{E} = 1/2(\mathbf{C} - \mathbf{I})$ ($[\mathbf{I}]$ is the identity tensor). Its components are as follows:

$$\begin{cases} E_{zz}=\psi+\dfrac{\psi^2}{2}+\dfrac{\varphi^2}{2}, \qquad E_{\theta\theta}=\dfrac{w+\psi z}{R(x)+z}+\dfrac{\left(w+\psi z\right)^2}{2\left(R(x)+z\right)^2}, \\ E_{xx}=u'+\dfrac{u'^2}{2}+\dfrac{w'^2}{2}+\left(\varphi'+u'\varphi'+w'\psi'\right)z+\left(\dfrac{\varphi'^2}{2}+\dfrac{\psi'^2}{2}\right)z^2, \\ \gamma_{zx}=2E_{zx}=\varphi+u'\varphi+w'+w'\psi+\left(\psi'+\psi\psi'+\varphi\varphi'\right)z \end{cases} \tag{6}$$

2.2. Hyperelastic FGM

Hyperelastics (as rubber-like materials) are kind of materials in which the stresses are only dependent on the initial and the final configurations but independent of the load path. The strain energy functions of these materials depend on the right Cauchy–Green deformation tensor through the strain invariants $\left(W^*(I_1,I_2,I_3)\right)$. In the present study, the hyperelastic material of the shell is assumed to be isotropic and non-homogenous with neo-Hookean material description in nearly incompressible condition which is a suitable hyperelastic model for rubbers and soft biological tissues. The response of neo-Hookean material to distortional part of the deformation has the following form [18, 22]:

$$W^*(I_1)=C_{1n}\left(I_1-3\right) \tag{7}$$

Here C_{1n} is material constant resulting from experimental tests. Non-homogenous and isotropic FG hyperelastic materials have different properties in terms of points. The variations of properties in functionally graded shells are generally considered in radial and/or longitudinal directions. As the constants of neo-Hookean model have relation with linear elastic shear modulus $C_{1n}=\mu_n/2$, the constant of this model could be considered with power-law distribution continuously and smoothly in the radial direction. Although the variations of the FG layers are the function of radial direction in the current research, the properties of outer points are determined based on thickness profile because of outer radius variation along axial direction. The FG material constant has the following form [20, 22]:

$$C_{1n}=C_1\left(\frac{R+z}{r_i}\right)^n \tag{8}$$

where C_1 is material constant fixed at the internal surface and n is the inhomogeneity index determined empirically. To properly deal with incompressibility condition, distortional part of the strain energy function W^* is classically augmented by two constraint terms; first constraint enforce incompressibility $\left(J=1\right)$ via a Lagrange multiplier (P) which can be identified as the hydrostatic pressure and the other one guarantee the stress free state of reference configuration with no physical meaning. Therefore, the following strain energy function could be demonstrated [3, 35]:

$$W\left(I_1,J\right)=W^*(I_1)+\frac{P}{2}(J-1)-P_0H(J) \tag{9}$$

In the present study, the extension of incompressible materials to nearly incompressible materials is considered. Indeed, the assumption of almost incompressible material is accomplished by dropping the restriction $J=1$ and including a hydrostatic work term in the strain energy function. The compressibility parameter k can be defined as the ratio of the volumetric stress, known as hydrostatic pressure (P), to the volumetric strain [2, 12].

$$k=\frac{P}{\Delta V/V_0}=\frac{P}{J-1} \tag{10}$$

V_0 and ΔV are the reference volume and volume changes through deformation, respectively. Considering k as an additional material constant, representing the bulk modulus, only scales the second term in Eq. (9) but does not change its shape [35, 36]. In this context k can be interpreted as the compressibility parameter that enforces incompressibility if large values are chosen. Although k can be estimated by volumetric experimental tests, some relations are recommended for estimating the value of incompressibility parameter; for instance $k=2\mu(1+\nu)/\left(3(1-2\nu)\right)$. The common part of similar relations is definition of the bulk modulus based on linear elastic shear modulus (μ) and Poisson's ratio (ν). In nearly incompressible materials such as rubbers or soft biological tissues, Poisson's ratio in regard to the intensity of compressibility has constant values about $\nu=0.49-0.499$. The order of graded compressibility parameter k_n (bulk modulus) can be estimated based on the intensity of compressibility in FG material as [7, 9, 35]:

$$\nu=0.49\rightarrow k_n\propto C_{1n}\times10^2 \quad \text{or} \quad \nu=0.499\rightarrow k_n\propto C_{1n}\times10^3 \tag{11}$$

Therefore, variation of bulk modulus can be considered similar to Eq. (8).

$$k_n\left(x,z\right)=k\left(\frac{R(x)+z}{r_i}\right)^n \tag{12}$$

where k is the bulk modulus fixed at the internal radius.

Considering zero values of displacement components in the reference configurations (initial state) with Eqs. (4) and (5) lead in $[\mathbf{F}]=[\mathbf{C}]=[\mathbf{I}]$ and $(I_1,I_2,I_3,J)=(3,3,1,1)$. In general state of nearly incompressible hyperelastic materials (as neo-Hookean ones), hydrostatic pressure $P=k(J-1)$ does not vanish even at the natural state. Therefore, constant P_0 and function $H(J)$, in the third term of the right hand side of Eq. (9), along with the condition $H(J)=0, H'(J)=1\Leftrightarrow J=1$ guarantee the stress free reference configuration. The first condition $(H(J)=0)$ corresponds to the incompressibility constraint $J=1$ while the second one $(H'(J)=1)$ is necessary for giving the meaning of pressure to the constant multiplier of H as $-P_0$. The initial value of P (i.e. P_0), with no clear physical meaning, should be determined to make the initial stress zero. In the current study, the function $H(J)$ are considered as [3, 35]:

$$H(J)=\ln(J) \tag{13}$$

Finally, the strain energy per unit undeformed volume of FG hyperelastic material for neo-Hookean model in nearly incompressible condition is expressed in the coupled form [1, 4].

$$W=C_{1n}\left(I_1-3\right)-P_{0n}\ln(J)+\frac{k_n}{2}\left(J-1\right)^2 \tag{14}$$

Constitutive equation of coupled neo-Hookean model in material description and nearly incompressible, isotropic and non-homogenous conditions is resulted consequently [37, 38].

$$\mathbf{S}=2\frac{\partial W}{\partial\mathbf{C}}=2C_{1n}\mathbf{I}+\left[k_nJ\left(J-1\right)-P_{0n}\right]\mathbf{C}^{-1} \tag{15}$$

Eq. (15) relates the right Cauchy–Green strain tensor $[\mathbf{C}]$ to the second Piola–Kirchhoff stress tensor $[\mathbf{S}]$ through constitutive relation. $[\mathbf{I}]$ is the identity tensor. The initial stress is zero if the hydrostatic pressure vanishes at the natural state, and vice versa. Recalling the assumption of stress-free reference configuration, Eq. (15) result in $P_{0n}=2C_{1n}=\mu_n$ [4, 5]. Thus, the multiplier P_{0n} in the case of $H(J)=\ln(J)$ denotes the pressure measured in the initial volume. The components in the right hand side of Eq. (15), other than identity tensor and material constants, can be written in the displacement field components. Therefore, the relation between the second Piola–Kirchhoff stress tensor and displacement components could be derived.

2.3. Governing equations

Based on the principle of virtual work, the variation of strain energy of the elastic body is equal to the variation of external work related to loading. The weak form of equilibrium equation, in quasi-static conditions with no body forces, can be written based on energy conjugate variables ($\mathbf{S}$ and $\mathbf{E}$) in deformed configuration [38-40].

$$-\iiint_{V_0} \mathbf{S} : \delta\mathbf{E}\, \mathrm{d}V_0 + \iint_{A_0} \mathbf{t}.\delta\mathbf{y}\, \mathrm{d}A_0 = 0 \tag{16}$$

where V_0 and A_0 are the volume and boundary of the volume in the undeformed configuration, respectively. Vector $\mathbf{t}$ denotes the traction applied to the boundary (pressure load), $\delta\mathbf{y}$ is the virtual displacement field and $\delta\mathbf{E}$ is the virtual strain field deduced from the gradient of $\mathbf{y}$. The variation of external work related to non-uniform internal pressure $P_{\mathrm{i}}(x)$ applied to the internal surface element $\mathrm{d}A_{\mathrm{i}}$ is:

$$\iint_{A_0} \mathbf{t}.\delta\mathbf{y}\, \mathrm{d}A_0 = \iint_{A_{\mathrm{i}}} P_{\mathrm{i}}(x)\, \delta U_{\mathrm{z}}\big|_{r=r_{\mathrm{i}}}\, \mathrm{d}A_{\mathrm{i}}, \qquad \mathrm{d}A_{\mathrm{i}} = 2\pi r_{\mathrm{i}}\, \mathrm{d}x \tag{17}$$

Above relation can be rewritten by considering displacement components from Eq. (3).

$$2\pi \int_0^L P_{\mathrm{i}}(x) \left(R(x) - \frac{h(x)}{2} \right) \left(\delta w - \frac{h(x)}{2} \delta\psi \right) \mathrm{d}x \tag{18}$$

The internal virtual work of the volume element $\mathrm{d}V_0$ can be expressed in material description.

$$\begin{cases} \iiint_{V_0} \mathbf{S} : \delta\mathbf{E}\, \mathrm{d}V_0 = \iiint_{V_0} S^{\mathrm{ij}}\, \delta E_{\mathrm{ij}}\, \mathrm{d}V_0, \\ \mathrm{d}V_0 = 2\pi r(x)\, \mathrm{d}r\, \mathrm{d}x = 2\pi \left(R(x) + \mathrm{z} \right) \mathrm{d}z\, \mathrm{d}x \end{cases} \tag{19}$$

The variation of strain energy can be derived based on non-zero physical components of second Piola–Kirchhoff stress as

$$\begin{aligned} 2\pi \int_0^L \int_{-h(x)/2}^{+h(x)/2} \Big[& S^{zz}\, \delta E_{zz} + S^{\theta\theta}\, \delta E_{\theta\theta} + S^{xx}\, \delta E_{xx} \\ & + S^{zx}\, \delta\gamma_{zx} \Big] R(x) \left(1 + \frac{z}{R(x)} \right) \mathrm{d}z\, \mathrm{d}x \end{aligned} \tag{20}$$

Considering Eq. (6) and variational principles, the variation of strain tensor components can be calculated.

$$\begin{cases} \delta E_{xx} = \delta u' + u'\delta u' + w'\delta w' + \left(\delta\varphi' + u'\delta\varphi' + \varphi'\delta u' + w'\delta\psi' \right. \\ \quad \left. + \psi'\delta w' \right) z + \left(\varphi'\delta\varphi' + \psi'\delta\psi' \right) z^2, \quad \delta E_{zz} = \delta\psi + \psi\delta\psi + \varphi\delta\varphi, \\ \delta E_{\theta\theta} = \dfrac{\left(\delta w + z\, \delta\psi \right)}{\left(R(x) + z \right)^2} \left(R(x) + z + w + \psi z \right) \\ \delta\gamma_{zx} = \delta\varphi + u'\delta\varphi + \varphi\delta u' + \delta w' + w'\delta\psi + \psi\delta w' \\ \quad + \left(\delta\psi' + \psi\delta\psi' + \psi'\delta\psi + \varphi\delta\varphi' + \varphi'\delta\varphi \right) z \end{cases} \tag{21}$$

The stress resultants are defined as follows:

$$\left\{ N_z \quad M_z \quad Q_z \right\}^{\mathrm{T}} = \int_{-h(x)/2}^{+h(x)/2} S^{zz} \left\{ 1 \quad z \quad z^2 \right\}^{\mathrm{T}} \left(1 + \frac{z}{R(x)} \right) \mathrm{d}z \tag{22}$$

$$\left\{ N_\theta \quad M_\theta \quad Q_\theta \right\}^{\mathrm{T}} = \int_{-h(x)/2}^{+h(x)/2} S^{\theta\theta} \left\{ 1 \quad z \quad z^2 \right\}^{\mathrm{T}} \mathrm{d}z \tag{23}$$

$$\left\{ N_\theta^* \quad M_\theta^* \quad Q_\theta^* \right\}^{\mathrm{T}} = \int_{-h(x)/2}^{+h(x)/2} S^{\theta\theta} \left\{ 1 \quad z \quad z^2 \right\}^{\mathrm{T}} \left(\frac{R(x)}{R(x) + z} \right) \mathrm{d}z \tag{24}$$

$$\left\{ N_x \quad M_x \quad Q_x \right\}^{\mathrm{T}} = \int_{-h(x)/2}^{+h(x)/2} S^{xx} \left\{ 1 \quad z \quad z^2 \right\}^{\mathrm{T}} \left(1 + \frac{z}{R(x)} \right) \mathrm{d}z \tag{25}$$

$$\left\{ N_{zx} \quad M_{zx} \quad Q_{zx} \right\}^{\mathrm{T}} = K_S \int_{-h(x)/2}^{+h(x)/2} S^{zx} \left\{ 1 \quad z \quad z^2 \right\}^{\mathrm{T}} \left(1 + \frac{z}{R(x)} \right) \mathrm{d}z \tag{26}$$

K_S is shear correction factor applied to the stress resultants related to shear stresses because of preventing stress overestimation. We consider $K_S = 5/6$ in the present study [26]. Substituting Eqs. (18) and (20) into Eq. (16), considering strain invariants from Eq. (21), multiplying the sides in $-r_{\mathrm{i}}^n$ and carrying out the integration by parts, the equilibrium equations of nonlinear hyperelastic cylindrical shell with variable thickness under non-uniform internal pressure are obtained.

$$\frac{\mathrm{d}}{\mathrm{d}x} \left[R(x) \left(N_x \left(1 + u' \right) + M_x \varphi' + N_{zx} \varphi \right) \right] = 0 \tag{27}$$

$$\begin{aligned} & \frac{\mathrm{d}}{\mathrm{d}x} \left[R(x) \left(M_x \left(1 + u' \right) + Q_x \varphi' + M_{zx} \varphi \right) \right] \\ & \quad - R(x) \left(N_z \varphi + N_{zx} \left(1 + u' \right) + M_{zx} \varphi' \right) = 0 \end{aligned} \tag{28}$$

$$\begin{aligned} & \frac{\mathrm{d}}{\mathrm{d}x} \left[R(x) \left(N_x w' + M_x \psi' + N_{zx} \left(1 + \psi \right) \right) \right] - N_\theta \\ & \quad - \frac{1}{R(x)} \left(N_\theta^* w + M_\theta^* \psi \right) = -P_{\mathrm{i}}(x) \left(R(x) - \frac{h(x)}{2} \right) \end{aligned} \tag{29}$$

$$\begin{aligned} & \frac{\mathrm{d}}{\mathrm{d}x} \left[R(x) \left(M_x w' + Q_x \psi' + M_{zx} \left(1 + \psi \right) \right) \right] - M_\theta \\ & \quad - R(x) \left(N_z \left(1 + \psi \right) + N_{zx} w' + M_{zx} \psi' \right) \\ & \quad - \frac{1}{R(x)} \left(M_\theta^* w + Q_\theta^* \psi \right) = P_{\mathrm{i}}(x) \frac{h(x)}{2} \left(R(x) - \frac{h(x)}{2} \right) \end{aligned} \tag{30}$$

3. Analytical solution

3.1. Perturbation theory

In current study, Match Asymptotic Expansion of the perturbation theory is used to solve the governing equations. Main advantage of this method is fast convergence in nonlinear problems. The governing equations (27)-(30) are a system of four nonlinear coupled differential equations with variable coefficients in cylinder with variable thickness. Preliminary definitions, simplifications and preparations are necessary for MAE usage. At first, it is necessary to convert the equations into dimensionless form by the following definitions [24, 41]:

$$\begin{cases} \bar{x} = \dfrac{x}{L}, \quad \bar{h} = \dfrac{h}{h_0}, \quad \bar{z} = \dfrac{z}{h_0}, \quad \bar{r}_{\mathrm{i}} = \dfrac{r_{\mathrm{i}}}{h_0}, \quad \bar{R} = \dfrac{R}{h_0}, \\ \bar{u} = \dfrac{u}{h_0}, \quad \bar{\varphi} = \varphi, \quad \bar{w} = \dfrac{w}{h_0}, \quad \bar{\psi} = \psi, \quad \varepsilon = \dfrac{h_0}{L}, \quad \bar{P}_{\mathrm{i}} = \dfrac{P_{\mathrm{i}} \bar{r}_{\mathrm{i}}^n}{\varepsilon} \end{cases} \tag{31}$$

The mark $\bar{}$ on the parameters denotes the dimensionless quantity. h_0 is the characteristic thickness which is commonly considered the minimal thickness of shell. ε is perturbation parameter which is assumed small quantity. The main idea of perturbation theory is that perturbation parameter is so small that coefficients of its different power don't have the same order which lead in equality of ε^{i} coefficients. Considering each coefficient results in displacement quasi-vector $\{\bar{\mathbf{y}}(\bar{x})\}$. Existence of two boundary layer lead in two region of solution near boundaries (inner solution) and a solution away from boundaries (outer solution) [41].

In shear deformation theory, the differentials and integrations are performed over $\bar{x}$ and $\bar{z}$ direction, respectively. Therefore, for simplification and abbreviation of representing equations, a dimensionless integration could be defined as follow:

$$\overline{II}\,(\mathrm{i},\mathrm{j})=\frac{II\,(\mathrm{i},\mathrm{j})}{h_0^{\,\mathrm{i}+\mathrm{j}+1}}=\int_{-\bar{h}(\bar{x})/2}^{+\bar{h}(\bar{x})/2}\bar{z}^{\,\mathrm{i}}\left(\bar{R}(\bar{x})+\bar{z}\right)^{\mathrm{j}}\mathrm{d}\,\bar{z} \tag{32}$$

which is the function of geometric parameters $\bar{R}(\bar{x})$, $\bar{h}(\bar{x})$ and inhomogeneity index n. The inverse of coefficient matrices will be needed in the next sections. Hence, Eq. (27) should be integrated. The constant of integration is $\bar{c}_0=c_0\bar{r}_{\mathrm{i}}^{\,n}/\varepsilon$ where ε is bookkeeping perturbed parameter. As there is no $\bar{u}$ in governing equations unlike $\mathrm{d}\bar{u}/\mathrm{d}\bar{x}$, parameter $\bar{v}=\varepsilon(\mathrm{d}\bar{u}/\mathrm{d}\bar{x})$ is considered instead. The unknown parameter $\bar{u}$ can be determined through the relation $\bar{u}=(1/\varepsilon)\int\bar{v}\,\mathrm{d}\,\bar{x}+c_7$ where c_7 is the constant of integration. $\bar{c}_0$ and c_7 will be calculated from boundary conditions.

The following parameters need to be defined in regard to material and geometrical constants C_1,C_2,k,K_s of internal layer because of abbreviation in representing inner and outer equations.

$$\begin{cases}\left(1-K_s\right)=\hat{K}_s, & 2C_1-k=Ck_1, \quad 4C_1-k=Ck_2,\\ 2C_1-3k=Ck_3, & 4C_1-5k=Ck_4, \quad 8C_1-7k=Ck_5\end{cases} \tag{33}$$

3.2. Outer solution

The outer expansion of solution is considered a uniform series of ε as $\bar{\mathbf{y}}_{\mathrm{O}}(\bar{x},\varepsilon)=\varepsilon\left(\bar{\mathbf{y}}_{\mathrm{O1}}(\bar{x})+\varepsilon\bar{\mathbf{y}}_{\mathrm{O2}}(\bar{x})\right)$. The subscript "O" stands for outer solution. Furthermore, the subscript "1" and "2" shows first and second order expansion, respectively. Substituting the outer expansion into governing equations and considering the terms with the same order of ε result in the first and second order equations of outer solution. In this section $(\,)'=\mathrm{d}(\,)/\mathrm{d}\bar{x}$.

$$\begin{cases}\mathrm{O}(\varepsilon^1):\left[\mathbf{A}_{\mathrm{O}}\right]\left\{\bar{\mathbf{y}}_{\mathrm{O1}}\right\}=\left\{\mathbf{F}_{\mathrm{O1}}\right\},\\ \mathrm{O}(\varepsilon^2):\left[\mathbf{A}_{\mathrm{O}}\right]\left\{\bar{\mathbf{y}}_{\mathrm{O2}}\right\}=\left\{\mathbf{F}_{\mathrm{O2}}\right\}, \quad \left\{\mathbf{F}_{\mathrm{O2}}\right\}=\left\{\mathbf{F}_{\mathrm{O2}}^{II}\right\}+\left\{\mathbf{F}_{\mathrm{O2}}^{II'}\right\}\end{cases} \tag{34}$$

Here $\left[\mathbf{A}_{\mathrm{O}}\right]$, $\left\{\mathbf{F}_{\mathrm{O1}}\right\}$ and $\left\{\mathbf{F}_{\mathrm{O2}}\right\}$ are coefficient matrices, non-homogeneity vectors of first and second order equation, respectively. $\left\{\bar{\mathbf{y}}_{\mathrm{Oi}}\right\}$ are unknown displacement vectors in "i"th-order of outer solution. $\left\{\mathbf{F}_{\mathrm{O2}}\right\}$ consist of two vectors $\left\{\mathbf{F}_{\mathrm{O2}}^{II}\right\}$ and $\left\{\mathbf{F}_{\mathrm{O2}}^{II'}\right\}$ correspond to $\overline{II}\,(\bar{x})$ and derivative of $\overline{II}\,(\bar{x})$, respectively. These vectors are defined in appendices. Other non-zero components of the mentioned matrix and vectors are

$$\left\{\bar{\mathbf{y}}_{\mathrm{O1}}\right\}=\left\{\bar{v}_{\mathrm{O1}},\bar{\varphi}_{\mathrm{O1}},\bar{w}_{\mathrm{O1}},\bar{\psi}_{\mathrm{O1}}\right\}^{\mathrm{T}}, \quad \left\{\bar{\mathbf{y}}_{\mathrm{O2}}\right\}=\left\{\bar{v}_{\mathrm{O2}},\bar{\varphi}_{\mathrm{O2}},\bar{w}_{\mathrm{O2}},\bar{\psi}_{\mathrm{O2}}\right\}^{\mathrm{T}} \tag{35}$$

$$\begin{cases}\left[\mathbf{A}_{\mathrm{O}}\right]_{11}=k\,\overline{II}\,(0,n+1), \quad \left[\mathbf{A}_{\mathrm{O}}\right]_{22}=-2K_sC_1\overline{II}\,(0,n+1),\\ \left[\mathbf{A}_{\mathrm{O}}\right]_{13}=-\left[\mathbf{A}_{\mathrm{O}}\right]_{31}=-Ck_2\overline{II}\,(0,n), \quad \left[\mathbf{A}_{\mathrm{O}}\right]_{33}=-k\,\overline{II}\,(0,n-1),\\ \left[\mathbf{A}_{\mathrm{O}}\right]_{14}=-\left[\mathbf{A}_{\mathrm{O}}\right]_{41}=-Ck_2\left(\overline{II}\,(1,n)+\overline{II}\,(0,n+1)\right),\\ \left[\mathbf{A}_{\mathrm{O}}\right]_{34}=\left[\mathbf{A}_{\mathrm{O}}\right]_{43}=Ck_2\overline{II}\,(0,n)-k\,\overline{II}\,(1,n-1),\\ \left[\mathbf{A}_{\mathrm{O}}\right]_{44}=Ck_2\overline{II}\,(1,n)-k\left(\overline{II}\,(0,n+1)+\overline{II}\,(2,n-1)\right)\end{cases} \tag{36}$$

$$\left\{\mathbf{F}_{\mathrm{O1}}\right\}=\begin{Bmatrix}\bar{c}_0/h_0^{\,2}\\ 0\\ -\bar{P}_{\mathrm{i}}(\bar{x})\left(\bar{R}(\bar{x})-\dfrac{\bar{h}(\bar{x})}{2}\right)\\ \bar{P}_{\mathrm{i}}(\bar{x})\left(\dfrac{\bar{R}(\bar{x})\bar{h}(\bar{x})}{2}-\dfrac{\bar{h}^2(\bar{x})}{4}\right)\end{Bmatrix} \tag{37}$$

The solutions of the algebraic equations (34) can be demonstrated as follows:

$$\left\{\bar{\mathbf{y}}_{\mathrm{O1}}\right\}=\left[\mathbf{A}_{\mathrm{O}}\right]^{-1}\left\{\mathbf{F}_{\mathrm{O1}}\right\}, \qquad \left\{\bar{\mathbf{y}}_{\mathrm{O2}}\right\}=\left[\mathbf{A}_{\mathrm{O}}\right]^{-1}\left\{\mathbf{F}_{\mathrm{O2}}\right\} \tag{38}$$

3.3. Inner solution

As the outer solutions don't satisfy the B.C., existence of boundary layers at $\bar{x}=0,1$ can be concluded. Therefore, fast variable $(\tilde{x}_\alpha)$ should be considered as a new variable for regions around boundaries. Considering fast variables make it possible to measure the great variation of mechanical response around boundaries.

$$\begin{cases}\bar{x}=0\to\alpha=0, \ \ \tilde{x}_0=\dfrac{\bar{x}}{\varepsilon} \quad \text{(left boundary)},\\ \bar{x}=1\to\alpha=1, \ \ \tilde{x}_1=\dfrac{(\bar{x}-1)}{\varepsilon} \quad \text{(right boundary)}\end{cases} \tag{39}$$

Subscript "$\alpha=0,1$" shows $\bar{x}=\alpha$ in the boundary. Perturbation parameter appears in new definition of differential over fast variables $\tilde{x}_\alpha$:

$$\frac{\mathrm{d}}{\mathrm{d}\,\tilde{x}_\alpha}=\varepsilon\frac{\mathrm{d}}{\mathrm{d}\,\bar{x}}, \quad \frac{\mathrm{d}^2}{\mathrm{d}\,\tilde{x}_\alpha^{\,2}}=\varepsilon^2\frac{\mathrm{d}^2}{\mathrm{d}\,\bar{x}^2} \tag{40}$$

In cylinder with variable thickness and non-uniform pressure, it is necessary to derive Taylor expansion for all the parameters of axial function $\bar{\Lambda}(\tilde{x})$ as

$$\bar{\Lambda}(\tilde{x})=\bar{\Lambda}_\alpha+\varepsilon\tilde{x}_\alpha\mathrm{D}\bar{\Lambda}_\alpha+\ldots \tag{41}$$

with $\bar{\Lambda}_\alpha=\bar{\Lambda}(\bar{x}=\alpha)$ and $\mathrm{D}\bar{\Lambda}_\alpha=\mathrm{d}\,\bar{\Lambda}(\bar{x})/\mathrm{d}\,\bar{x}\big|_{\bar{x}=\alpha}$ definition. $\bar{x}$ is substituted by new fast variable of inner expansion $(\tilde{x}_\alpha)$. Taylor expansion should be written for the following parameters:

$$\begin{cases}\bar{h}(\tilde{x})=\bar{h}_\alpha+\varepsilon\tilde{x}_\alpha\mathrm{D}\bar{h}_\alpha, \quad \bar{R}(\tilde{x})=\bar{R}_\alpha+\varepsilon\tilde{x}_\alpha\mathrm{D}\bar{R}_\alpha,\\ \bar{P}_{\mathrm{i}}(\tilde{x})=\bar{P}_{\mathrm{i}\alpha}+\varepsilon\tilde{x}_\alpha\mathrm{D}\bar{P}_{\mathrm{i}\alpha}, \quad \overline{II}_\alpha(\tilde{x})=\overline{II}_\alpha+\varepsilon\tilde{x}_\alpha\mathrm{D}\overline{II}_\alpha\end{cases} \quad (\alpha=0,1) \tag{42}$$

Substituting inner expansion $\bar{\mathbf{y}}_\alpha(\tilde{x}_\alpha,\varepsilon)=\varepsilon\left(\bar{\mathbf{y}}_{\alpha1}(\tilde{x}_\alpha)+\varepsilon\bar{\mathbf{y}}_{\alpha2}(\tilde{x}_\alpha)\right)$ into governing equations with mentioned changes in section 3.1 and considering terms with the same order of ε result in inner equations at boundary α:

$$\begin{cases}\mathrm{O}(\varepsilon^1):\left[\mathbf{A}_{\alpha1}\right]\dfrac{\mathrm{d}^2}{\mathrm{d}\,\tilde{x}_\alpha^{\,2}}\left\{\bar{\mathbf{y}}_{\alpha1}\right\}+\left[\mathbf{A}_{\alpha2}\right]\dfrac{\mathrm{d}}{\mathrm{d}\,\tilde{x}_\alpha}\left\{\bar{\mathbf{y}}_{\alpha1}\right\}+\left[\mathbf{A}_{\alpha3}\right]\left\{\bar{\mathbf{y}}_{\alpha1}\right\}=\left\{\mathbf{F}_{\alpha1}\right\}\\ \mathrm{O}(\varepsilon^2):\left[\mathbf{A}_{\alpha1}\right]\dfrac{\mathrm{d}^2}{\mathrm{d}\,\tilde{x}_\alpha^{\,2}}\left\{\bar{\mathbf{y}}_{\alpha2}\right\}+\left[\mathbf{A}_{\alpha2}\right]\dfrac{\mathrm{d}}{\mathrm{d}\,\tilde{x}_\alpha}\left\{\bar{\mathbf{y}}_{\alpha2}\right\}+\left[\mathbf{A}_{\alpha3}\right]\left\{\bar{\mathbf{y}}_{\alpha2}\right\}=\left\{\mathbf{F}_{\alpha2}\right\}\\ \left\{\mathbf{F}_{\alpha2}\right\}=\left\{\mathbf{F}_{\alpha2}^{II\alpha}\right\}+\left\{\mathbf{F}_{\alpha2}^{\mathrm{DA}\alpha}\right\}+\left\{\mathbf{F}_{\alpha2}^{\mathrm{D}II\alpha}\right\}+\left\{\mathbf{F}_{\alpha2}^{P_\alpha}\right\}+\left\{\mathbf{F}_{\alpha2}^{\mathrm{DP}\alpha}\right\}\end{cases} \tag{43}$$

$\left[\mathbf{A}_{\alpha1}\right]$, $\left[\mathbf{A}_{\alpha2}\right]$ and $\left[\mathbf{A}_{\alpha3}\right]$ are coefficient matrices at the boundary α. $\left\{\mathbf{F}_{\alpha1}\right\}$ and $\left\{\mathbf{F}_{\alpha2}\right\}$ are the non-homogeneity vectors of differential equation at the first and second order equation of boundary α, respectively. $\left\{\bar{\mathbf{y}}_{\alpha\mathrm{i}}\right\}$ are unknown displacement vectors in "i"th-order of inner solution at the boundary α. $\left\{\mathbf{F}_{\alpha2}^{II\alpha}\right\}$ and $\left\{\mathbf{F}_{\alpha2}^{\mathrm{D}II\alpha}\right\}$, in vector $\left\{\mathbf{F}_{\alpha2}\right\}$, are related to $\overline{II}_\alpha(\tilde{x})$ and $\mathrm{D}\overline{II}_\alpha(\tilde{x})$ (in Taylor expansion), respectively. $\left\{\mathbf{F}_{\alpha2}^{\mathrm{DA}\alpha}\right\}$, derived in non-homogeneity of second order equation, is resulted from Taylor expansion of coefficient matrices related to first order equation. $\left\{\mathbf{F}_{\alpha2}^{P_\alpha}\right\}$ and $\left\{\mathbf{F}_{\alpha2}^{\mathrm{DP}\alpha}\right\}$, related to $\bar{P}_{\mathrm{i}\alpha}(\tilde{x}_\alpha)$ and $\mathrm{D}\bar{P}_{\mathrm{i}\alpha}(\tilde{x}_\alpha)$ (in Taylor expansion of pressure), are derived from variable thickness and non-uniform pressure, respectively. The components of $\left\{\mathbf{F}_{\alpha2}\right\}$ will be defined in appendices. Other non-zero components of the matrices and vectors are defined below. $(\,)'=\mathrm{d}(\,)/\mathrm{d}\tilde{x}_\alpha$ is defined for the inner expansion of boundary α.

$$\left\{\bar{\mathbf{y}}_{\alpha1}\right\}=\left\{\bar{v}_{\alpha1},\bar{\varphi}_{\alpha1},\bar{w}_{\alpha1},\bar{\psi}_{\alpha1}\right\}^{\mathrm{T}}, \qquad \left\{\bar{\mathbf{y}}_{\alpha2}\right\}=\left\{\bar{v}_{\alpha2},\bar{\varphi}_{\alpha2},\bar{w}_{\alpha2},\bar{\psi}_{\alpha2}\right\}^{\mathrm{T}} \tag{44}$$

$$\begin{cases}\left[\mathbf{A}_{\alpha1}\right]_{22}=k\,\overline{II}_\alpha(2,n+1), \quad \left[\mathbf{A}_{\alpha1}\right]_{33}=2K_sC_1\overline{II}_\alpha(0,n+1)\\ \left[\mathbf{A}_{\alpha1}\right]_{34}=\left[\mathbf{A}_{\alpha1}\right]_{43}=2K_sC_1\overline{II}_\alpha(1,n+1),\\ \left[\mathbf{A}_{\alpha1}\right]_{44}=2K_sC_1\overline{II}_\alpha(2,n+1)\end{cases} \tag{45}$$

$$\begin{cases}\left[\mathbf{A}_{\alpha 2}\right]_{12}=\left[\mathbf{A}_{\alpha 2}\right]_{21}=k\,\overline{\Pi}_{\alpha}(1,n+1),\\ \left[\mathbf{A}_{\alpha 2}\right]_{23}=-\left[\mathbf{A}_{\alpha 2}\right]_{32}=-2K_sC_1\overline{\Pi}_{\alpha}(0,n+1)-Ck_2\overline{\Pi}_{\alpha}(1,n)\\ \left[\mathbf{A}_{\alpha 2}\right]_{24}=-\left[\mathbf{A}_{\alpha 2}\right]_{42}=-2K_sC_1\overline{\Pi}_{\alpha}(1,n+1)-Ck_2\left(\overline{\Pi}_{\alpha}(2,n)+\overline{\Pi}_{\alpha}(1,n+1)\right)\end{cases} \quad (46)$$

$$\begin{cases}\left[\mathbf{A}_{\alpha 3}\right]_{11}=k\,\overline{\Pi}_{\alpha}(0,n+1),\quad \left[\mathbf{A}_{\alpha 3}\right]_{22}=-2K_sC_1\overline{\Pi}_{\alpha}(0,n+1),\\ \left[\mathbf{A}_{\alpha 3}\right]_{13}=-\left[\mathbf{A}_{\alpha 3}\right]_{31}=-Ck_2\overline{\Pi}_{\alpha}(0,n),\ \left[\mathbf{A}_{\alpha 3}\right]_{33}=-k\,\overline{\Pi}_{\alpha}(0,n-1)\\ \left[\mathbf{A}_{\alpha 3}\right]_{14}=-\left[\mathbf{A}_{\alpha 3}\right]_{41}=-Ck_2\left(\overline{\Pi}_{\alpha}(0,n+1)+\overline{\Pi}_{\alpha}(1,n)\right),\\ \left[\mathbf{A}_{\alpha 3}\right]_{34}=\left[\mathbf{A}_{\alpha 3}\right]_{43}=Ck_2\overline{\Pi}_{\alpha}(0,n)-k\,\overline{\Pi}_{\alpha}(1,n-1),\\ \left[\mathbf{A}_{\alpha 3}\right]_{44}=2Ck_2\overline{\Pi}_{\alpha}(1,n)-k\left(\overline{\Pi}_{\alpha}(0,n+1)+\overline{\Pi}_{\alpha}(2,n-1)\right)\end{cases} \quad (47)$$

$$\left\{\mathbf{F}_{\alpha 1}\right\}=\begin{Bmatrix}\bar{c}_0/h_0^{\,2}\\ 0\\ -\bar{P}_{i\alpha}\left(\bar{R}_\alpha-\dfrac{\bar{h}_\alpha}{2}\right)\\ \bar{P}_{i\alpha}\left(\dfrac{\bar{R}_\alpha\bar{h}_\alpha}{2}-\dfrac{\bar{h}_\alpha^2}{4}\right)\end{Bmatrix} \quad (48)$$

Eqs. (43) are systems of coupled non-homogenous differential equations with constant coefficients. Each equation has general $\left(\{\ \}_{\text{gen.}}\right)$ and particular $\left(\{\ \}_{\text{par.}}\right)$ solution:

$$\left\{\bar{\mathbf{y}}_{\alpha 1}\right\}=\left\{\bar{\mathbf{y}}_{\alpha 1}\right\}_{\text{gen.}}+\left\{\bar{\mathbf{y}}_{\alpha 1}\right\}_{\text{par.}},\qquad \left\{\bar{\mathbf{y}}_{\alpha 2}\right\}=\left\{\bar{\mathbf{y}}_{\alpha 2}\right\}_{\text{gen.}}+\left\{\bar{\mathbf{y}}_{\alpha 2}\right\}_{\text{par.}} \quad (49)$$

Considering m_α and $\{V_\alpha\}$ as eigenvalues and eigenvectors, respectively, and substituting general solution of exponential form $\left\{\bar{\mathbf{y}}_\alpha\right\}_{\text{gen.}}=\{V_\alpha\}\exp(m_\alpha\tilde{x}_\alpha)$ into homogenous part of Eqs. (43) lead in an eigenvalue problem:

$$\left(\left[\mathbf{A}_{\alpha 1}\right]m_\alpha^{\,2}+\left[\mathbf{A}_{\alpha 2}\right]m_\alpha+\left[\mathbf{A}_{\alpha 3}\right]\right)\{V_\alpha\}=\{0\} \quad (50)$$

The necessary condition for existing the solution of Eq. (50) is zero value of the coefficient determinant which is known as the characteristic equation of the system. Six non-zero roots of characteristic equation are the eigenvalues $(m_{\alpha i})$. Substituting roots into Eq. (50) lead in corresponding eigenvectors $(V_{\alpha i})$. The eigenvalues and eigenvectors are complex conjugate. Considering Van-Dyke's matching principle [41], the solution should be finite at $\tilde{x}_\alpha\to\infty$. Thus, eigenvalues with positive real part in left boundary $(\alpha=0)$ and negative real part in right boundary $(\alpha=1)$ are omitted. The general solution of boundary α can be calculated.

$$\left\{\bar{\mathbf{y}}_{\alpha 1}\right\}_{\text{gen.}}=\left\{\bar{\mathbf{y}}_{\alpha 2}\right\}_{\text{gen.}}=\left\{\bar{\mathbf{y}}_{\alpha}\right\}_{\text{gen.}}=\sum_{i=1}^{3}c_{\alpha i}\{V_{\alpha i}\}\exp(m_{\alpha i}\tilde{x}_\alpha) \quad (51)$$

Here $c_{\alpha i}(i=1,2,3)$ are three constants of boundary α defined by boundary conditions. The particular solution of Eq. (43), related to first order equation, is simply calculated by $\left\{\bar{\mathbf{y}}_{\alpha 1}\right\}_{\text{par.}}=\left[\mathbf{A}_{\alpha 3}\right]^{-1}\left\{\mathbf{F}_{\alpha 1}\right\}$. After the substitution of first order solution into second order one, $\left\{\mathbf{F}_{\alpha 2}\right\}$ is consist of nonlinear polynomial terms $\left(\{\ \}^{\text{pol.}}\right)$ and exponential terms by the equal roots $(\exp(m_{\alpha i}\tilde{x}_\alpha))$ and unequal roots $(\exp(q_{\alpha j}\tilde{x}_\alpha))$ with characteristic equations. Therefore, the particular solution of $O(\varepsilon^2)$ can be calculated by undetermined coefficients method as

$$\begin{cases}\left\{\bar{\mathbf{y}}_{\alpha 2}\right\}_{\text{par.}}=\left\{\bar{\mathbf{y}}_{\alpha 2}\right\}_{\text{par.}}^{\text{pol.}}+\left\{\bar{\mathbf{y}}_{\alpha 2}\right\}_{\text{par.}}^{\exp(m_i).}+\left\{\bar{\mathbf{y}}_{\alpha 2}\right\}_{\text{par.}}^{\exp(q_i).},\\ \left\{\bar{\mathbf{y}}_{\alpha 2}\right\}_{\text{par.}}^{\text{pol.}}=\left\{B_2\right\}\tilde{x}^2+\left\{B_1\right\}\tilde{x}+\left\{B_0\right\}\\ \left\{\bar{\mathbf{y}}_{\alpha 2}\right\}_{\text{par.}}^{\exp(mi).}=\sum_i\left(\left\{B_2\right\}_{mi}\tilde{x}^2+\left\{B_1\right\}_{mi}\tilde{x}+\left\{B_0\right\}_{mi}\right)\exp(m_{\alpha i}\tilde{x}_\alpha)\\ \left\{\bar{\mathbf{y}}_{\alpha 2}\right\}_{\text{par.}}^{\exp(qj).}=\sum_j\left(\left\{B_2\right\}_{qj}\tilde{x}^2+\left\{B_1\right\}_{qj}\tilde{x}+\left\{B_0\right\}_{qj}\right)\exp(q_{\alpha j}\tilde{x}_\alpha)\end{cases} \quad (52)$$

subscript "i" and "j" show the number of equal and unequal roots with characteristic equations. Undetermined coefficients $\{B_0\}$, $\{B_1\}$ and $\{B_2\}$ can be calculated by substituting $\left\{\bar{\mathbf{y}}_{\alpha 2}\right\}_{\text{par.}}$ into Eq. (43) - $O(\varepsilon^2)$.

3.4. Composite solution

In the MAE method, the composite solution $\left(\left\{\bar{\mathbf{y}}_{\text{comp.}}\right\}\right)$ is the summation of three calculated expansions (one outer solution $\left\{\bar{\mathbf{y}}_O\right\}$ and two inner ones $\left\{\bar{\mathbf{y}}_{\alpha=0}\right\},\left\{\bar{\mathbf{y}}_{\alpha=1}\right\}$) minus the overlapped parts of them. Outer solution around $\bar{x}\to 0,1$ overlap with inner solutions over $\tilde{x}_\alpha\to\pm\infty$ in a way that the common parts are removed from composite solution. Therefore,

$$\left\{\bar{\mathbf{y}}_{\text{comp.}}\right\}=\left\{\bar{\mathbf{y}}_{\text{O}}\right\}+\left\{\bar{\mathbf{y}}_{\alpha=0}\right\}+\left\{\bar{\mathbf{y}}_{\alpha=1}\right\}-\left\{\bar{\mathbf{y}}_{\text{O}}^{\alpha=0}\right\}-\left\{\bar{\mathbf{y}}_{\text{O}}^{\alpha=1}\right\} \quad (53)$$

where $\left\{\bar{\mathbf{y}}_{\text{O}}^{\alpha=0}\right\}$ and $\left\{\bar{\mathbf{y}}_{\text{O}}^{\alpha=1}\right\}$ are common parts of inner and outer solutions at two ends of the shell which can be determined by Van-Dyke's matching principle [41]. Eight constants, consist of three constants in general solution of each boundary and two constants $\bar{c}_0$ and c_7 should be calculated by the boundary conditions. The clamped boundary conditions in "i"th-order solution are:

$$\bar{x}=0,1\ \left(\tilde{x}_{0,1}=0\right)\rightarrow\bar{u}_{\alpha i},\bar{\varphi}_{\alpha i},\bar{w}_{\alpha i},\bar{\psi}_{\alpha i}=0\quad(i=1,2) \quad (54)$$

The unknown vector consists of dimensionless displacement field components $\{\bar{\mathbf{y}}\}=\left\{\bar{\mathbf{y}}_{\text{comp.}}\right\}=\{\bar{u},\bar{\varphi},\bar{w},\bar{\psi}\}$ would be obtained in terms of $\bar{x}$ and $\bar{z}$ variables. Considering Eq. (3) and definition $\bar{U}_{z,x}=U_{z,x}/h_0$, the dimensionless radial and axial displacements can be obtained. Using Eqs. (4-6) would yield $[\mathbf{F}],[\mathbf{C}],I_{1,2,3},J$ and $[\mathbf{E}]$, respectively. The hydrostatic pressure and second Piola–Kirchhoff stress distribution are also calculated by using Eqs. (10) and (15), respectively. Cauchy stress components can be defined by $[\boldsymbol{\sigma}]=(1/J)[\mathbf{F}][\mathbf{S}][\mathbf{F}]^{\text{T}}$ relation. The mathematical program of analytical solution has been written in MAPLE 18 software.

4. Results and discussion

4.1. Finite Element Modeling

In order to validate presented analytical solution and compare the results of pressurized thick cylinder with variable thickness made of nearly compressible FG hyperelastic material, a numerical solution based on finite element method is investigated. The ANSYS 16 package is used in the static analysis of thick hollow cylinder with variable thickness under non-uniform internal pressure. The PLANE183 element in the axisymmetric mode, which is an element with eight nodes and two translational degrees of freedom in the axial and radial directions per each node, has been used to model the mechanical part of the analysis. It has also mixed formulation capability for simulating deformations of nearly incompressible hyperelastic materials. The cylinder with variable thickness consists of some coherent homogeneous layers which properties, at the contact location of the layers, are the average of left and right limit of two layer boundaries. In order to model FG hyperelastic cylinder, an innovative application for multilayering the thickness in the axial direction has been performed. Homogenous layers with identical thickness and step-variable properties have been merged by this method. In order to consider neo-Hookean elastic model in nearly incompressible condition for each homogenous layer, two constants including μ and d should be defined for ANSYS software. The constant μ related to C_{1n} could be calculated from Eq. (8) in each layer. d is material incompressibility parameter by relation with bulk modulus as $k_n.d=2$ [8] which could be calculated from Eq. (12) in each layer. For non-uniform internal pressure, the pressure functions have been defined and applied to the internal layer nodes. Clamped boundary conditions have been exerted by preventing the nodes around the two ends of the cylinder from

movement. The numerical results (FEM) and analytical results (MAE) have been investigated for different case studies in the next sections.

4.2. Case studies

In order to illustrate the effects of material constant, gradient index, thickness profile type and pressure loading distribution on the mechanical behavior of hyperelastic pressure vessel, thick cylindrical shell with various non-uniform thickness and internal pressure profiles made of different materials constants and inhomogeneity index have been studied. In these case studies, unless otherwise notified, constant geometry parameters are considered as $r_i = 47\,\text{mm}$ and $L = 400\,\text{mm}$. Clamped boundary conditions are applied to the ends of the shell. The materials are assumed to be functionally graded hyperelastic ones with neo-Hookean model in nearly incompressible conditions. During the computation of numerical results, different material contestants according to various references presented in Table 1 are considered. The material constants are considered based on two state: 1) mentioned directly in these articles or 2) determined by authors from different test results (mentioned in these references) using least square method. The material parameters of FG neo-Hookean model are fixed at the internal surface. Authors consider $k = 10$ MPa for the cases with no compressibility parameter determination in Table 1 [9, 42].

Table 1. The characteristic of material constants.

Material Constants ID	Ref.	μ (MPa)	k (MPa)	Material Sample
MC_1	[9]	1.55	10	Rubbers
MC_2	[2, 7]	1.38	10	Rubber seals
MC_3	[8]	1.13	9.3	TDM 600
MC_4	[13]	0.90	10	Aneurysmal Abdominal Artery
MC_5	[18]	0.82	10	Vulcanized rubbers
MC_6	[43]	0.662	10	Natural gum rubbers
MC_7	[21]	0.398	10	Silicone rubbers
MC_8	[42]	0.346	10.5	Silicone elastomers

Internal pressure distribution and thickness profile varies non-uniformly along axial direction of the shell. Various pressure profiles are applied to the cylindrical shell in the range of $5\,\text{kPa} - 13\,\text{kPa}$. Dimensionless Cauchy stresses and hydrostatic pressure are defined as:

$$\bar{\boldsymbol{\sigma}} = \frac{\boldsymbol{\sigma}}{P_{i0}}, \quad \bar{P} = \frac{P}{P_{i0}} \tag{55}$$

P_{i0} is considered $9\,\text{kPa}$ which is the average of maximum and minimum pressure distributions. The variations of thickness profiles are in the range of $6\,\text{mm} - 12\,\text{mm}$. Tables 2 and 3 show the characteristic of applied non-uniform pressure and thickness profiles, respectively. Distribution of non-uniform thickness functions along axial direction are depicted in Fig. 2.

As current research studies the manner of pressurized rubber vessels in dimensionless state, the results of FSDT and MAE solution may be suitable for investigating some case studies of blood vessels. In particular, authors use proposed method to examine the inflation of a cylindrical tube at various internal pressure profiles and to compute the evolution of the inner radius (critical layer) under the internal pressure. Although the material models of blood vessels such as arteries have commonly exponential form to model the stiffening of the soft tissues, simple model such as neo-Hookean one is considered in numerous research for isotropic parts of blood vessels [14, 44]. Hence, case studies with variable thickness and pressure are selected similar to that of common elastic arteries (as unite layer) in current research in order to cover pressure vessels to blood vessels. The thick and thin parts of the vessels cover the average thickness of the layers in common elastic arteries. The pressure profiles vary in the range of $5\,\text{kPa}(40\,\text{mmHg}) - 13\,\text{kPa}(100\,\text{mmHg})$ which are the mean pressures of blood vessels related to human soft tissues. $100\,\text{mmHg}$ is the mean of systolic/diastolic pressure and $40\,\text{mmHg}$ may be occurred in hypotension pressure of arteries [45, 46]. Considering the applicability of the rubber elasticity theory to aortic soft tissues as one layer or multilayer vessel with variable material properties along thickness, the behavior of blood vessels under non-uniform pressure distribution could be demonstrated from current research. Furthermore, current study will present helpful results for estimating the wall degeneration of arteries within the aneurysm wall that affects the thickness profile of the tissue, which can be mostly analyzed as variable thickness blood vessels [11, 44].

Table 2. The characteristic of non-uniform internal pressure profiles.

Pressure Profile ID	Pressure Profile Function	Load Constants (kPa)
P_{i0}	$P_i(\bar{x}) = P_{i0} = \text{constant}$	$P_{i0} = 9$
P_{i1}	$P_i(\bar{x}) = P_a - (P_a - P_b)\bar{x}$	$P_a = 13,\ P_b = 5$
P_{i2}	$P_i(\bar{x}) = P_a - (P_a - P_b)\bar{x}^2$	$P_a = 13,\ P_b = 5$
P_{i3}	$P_i(\bar{x}) = P_a - (P_a - P_b)\bar{x}^3$	$P_a = 13,\ P_b = 5$
P_{i4}	$P_i(\bar{x}) = P_a - 4(P_a - P_{ab})(\bar{x} - \bar{x}^2)$	$P_a = P_b = 5,\ P_{ab} = 13$
P_{i5}	$P_i(\bar{x}) = P_a - (P_a - P_{ab})\sin(\pi\bar{x})$	$P_a = P_b = 13,\ P_{ab} = 5$

Table 3. The characteristic of non-uniform thickness profiles.

Thickness Profile ID	Thickness Profile Function	Geometry Constants (mm)
h_0	$h(\bar{x}) = h_0 = \text{constant}$	$h_0 = 6$
h_1	$h(\bar{x}) = h_a - (h_a - h_b)\bar{x}$	$h_a = 12,\ h_b = 6$
h_2	$h(\bar{x}) = h_a - (h_a - h_b)\bar{x}^2$	$h_a = 12,\ h_b = 6$
h_3	$h(\bar{x}) = h_a - (h_a - h_b)\bar{x}^3$	$h_a = 12,\ h_b = 6$
h_4	$h(\bar{x}) = h_a - 4(h_a - h_{ab})(\bar{x} - \bar{x}^2)$	$h_a = h_b = 6,\ h_{ab} = 12$
h_5	$h(\bar{x}) = h_a - (h_a - h_{ab})\sin(\pi\bar{x})$	$h_a = h_b = 12,\ h_{ab} = 6$

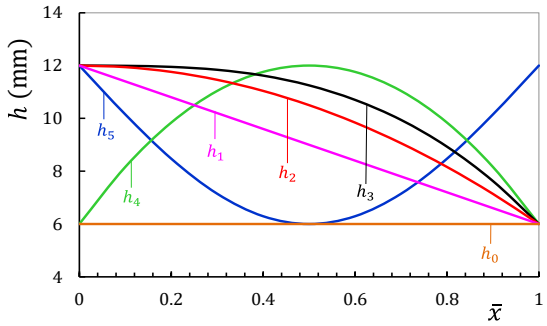

Figure 2. Distribution of non-uniform thickness functions along axial direction.

4.3. Effect of material constants and inhomogeneity index

In order to investigate the material constants effect on the approximation of the current solution and behaviour of shell, maximum values of radial and axial displacements for different material constants resulted from FSDT and FEM is presented in Tables 4 and 5. As the maximum values of displacements and maximum difference of analytical and numerical analysis in pressure vessels occur at the internal layer, the results of Tables 4 and 5 define the validity range of the proposed solution. Material constants, applied pressures and geometry of the cylinder are considered in the range of $5 < \bar{R} < 20$ and $1/400 < P_i/\mu < 1/100$ [10, 20, 46]. The difference percentage of dimensionless radial and axial displacement resulting from the numerical and analytical solution i.e. $\mathrm{Diff}\,\bar{U}_{z,x}(\%) = \left|\left(\bar{U}_{z,x}^{\mathrm{MAE}} - \bar{U}_{z,x}^{\mathrm{FEM}}\right)/\bar{U}_{z,x}^{\mathrm{FEM}}\right| \times 100$ for mentioned $\bar{R}$ and P_i/μ are less than 10%. For $\bar{R}$ values of more than 20 (thickness limit for thick cylinder) and less than 3 (very thick shells) solution accuracy may decrease. In fact, accuracy of MAE descend for great values of $\bar{R}$ because of intensifying nonlinear behavior of the cylinder while for small $\bar{R}$, the accuracy of shear deformation theory decrease in analyzing thick cylindrical shells. Ascending $\bar{R}$ lead in higher deformations and lower effect of clamped conditions on deformations and the peak points of displacements occurs far away from boundaries. An increase in P_i/μ and k or decrease in μ ascend displacement values and nonlinearity while descend the accuracy. However, descending μ values, for an equal ratio of P_i/μ, decrease displacements.

In order to show the displacements and stresses distribution in FG hyperelastic cylinder with variable thickness under non-uniform internal pressure, linear increase of thickness through $\bar{x}$ direction is considered proportional to linear pressure profile with positive inhomogeneity index $(n = 2)$. The material constants MC_2 are considered for FG neo-Hookean model. The distribution of dimensionless displacements resulted from FSDT and FEM are plotted in Fig. 3 at different layers. Because of greater radial displacements around left boundary, it can be concluded that pressure profile is more effective than thickness variation on shell displacement. According to Fig. 3(b), the axial displacement at points away from the boundaries is nearly independent from radius. Layers close to maximum pressure and clamped conditions are in axial tension; therefore, axial compression is dominants at the shell except in $\bar{z} \le 0$ around left boundary. Fig. 4 shows dimensionless Cauchy stress and hydrostatic pressure at different layers along axial direction. Circumferential and axial stresses (Fig. 4(a and b)), similar to hydrostatic pressure (Fig. 4(d)) as an average of principal stresses, have positive values in nearly all points of the shell except around boundaries at the outer layer away from loading. The reason is that the elements are in tensile state, but clamped conditions near boundaries at the layer away from loading cause resistance against displacement which lead in compressive stresses. In this state, inner layer of the shell in contact with pressure load have higher displacements and stresses than others. It is obviously observed that the circumferential stress is the largest component of the stress at points away from the boundaries while around the boundaries, the axial stress is the largest one. Existence of shear stress near boundaries (Fig. 4(c)) reveals the advantage of shear deformation theory respect to theories that neglect shear stress effect. Non-uniform peaks of displacements and stresses appear at the points away from boundaries where no shear stresses exist. Difference of MAE and FEM results increase at the points of internal and external layers away from boundaries. Although FSDT is suitable for displacement analysis rather than stress one, the results of MAE are more realistic around boundaries respect to FE solution. Fig. 5 shows the effect of MAE order on approximating the radial Cauchy stress distribution of middle layer. It can be concluded that $\mathrm{O}(\varepsilon^1)$ solution is suitable for linear analysis while $\mathrm{O}(\varepsilon^2)$ have acceptable approximation for problems with nonlinear kinematics and constitutive relations.

Table 4. Analytical and numerical values of maximum radial displacements for different material constants.

Mat. ID	$\bar{U}_z$,max	$P_i/\mu = 1/100$			$P_i/\mu = 1/200$			$P_i/\mu = 1/400$		
		$\bar{R}=5$	$\bar{R}=10$	$\bar{R}=20$	$\bar{R}=5$	$\bar{R}=10$	$\bar{R}=20$	$\bar{R}=5$	$\bar{R}=10$	$\bar{R}=20$
MC_1	FSDT	0.0792	0.3192	1.2895	0.0393	0.1587	0.6324	0.0196	0.0778	0.3100
	FEM	0.0799	0.3207	1.3038	0.0394	0.1579	0.6325	0.0195	0.0777	0.3099
MC_2	FSDT	0.0770	0.3144	1.3093	0.0388	0.1561	0.6230	0.0193	0.0770	0.3067
	FEM	0.0791	0.3174	1.3327	0.0387	0.1553	0.6244	0.0192	0.0769	0.3059
MC_3	FSDT	0.0768	0.3102	1.2550	0.0382	0.1538	0.6164	0.0191	0.0766	0.3049
	FEM	0.0778	0.3126	1.3053	0.0383	0.1536	0.6173	0.0190	0.0767	0.3024
MC_4	FSDT	0.0745	0.3023	1.2545	0.0371	0.1497	0.5992	0.0184	0.0745	0.2980
	FEM	0.0764	0.3039	1.2809	0.0378	0.1489	0.6020	0.0186	0.0744	0.2955
MC_5	FSDT	0.0738	0.3002	1.2171	0.0367	0.1487	0.5956	0.0183	0.0740	0.2961
	FEM	0.0761	0.3052	1.2461	0.0374	0.1491	0.5977	0.0184	0.0741	0.2937
MC_6	FSDT	0.0723	0.2961	1.2034	0.0359	0.1465	0.5897	0.0179	0.0721	0.2915
	FEM	0.0758	0.3016	1.2458	0.0371	0.1475	0.5909	0.0182	0.0723	0.2901
MC_7	FSDT	0.0694	0.2901	1.1852	0.0346	0.1434	0.5798	0.0172	0.0713	0.2876
	FEM	0.0730	0.2952	1.2312	0.0366	0.1440	0.5799	0.0178	0.0716	0.2848
MC_8	FSDT	0.0680	0.2899	1.1787	0.0338	0.1426	0.5733	0.0168	0.0705	0.2856
	FEM	0.0728	0.2947	1.2260	0.0357	0.1430	0.5754	0.0174	0.0713	0.2824

Table 5. Analytical and numerical values of maximum axial displacements for different material constants.

Mat. ID	$\bar{U}_{x,\max}$	$P_i/\mu = 1/100$			$P_i/\mu = 1/200$			$P_i/\mu = 1/400$		
		$\bar{R}=5$	$\bar{R}=10$	$\bar{R}=20$	$\bar{R}=5$	$\bar{R}=10$	$\bar{R}=20$	$\bar{R}=5$	$\bar{R}=10$	$\bar{R}=20$
MC_1	FSDT	0.0154	0.0469	0.1023	0.0078	0.0249	0.0632	0.0039	0.0122	0.0343
	FEM	0.0159	0.0476	0.1089	0.0080	0.0250	0.0637	0.0040	0.0126	0.0343
MC_2	FSDT	0.0153	0.0463	0.1018	0.0077	0.0245	0.0626	0.0039	0.0119	0.0336
	FEM	0.0158	0.0474	0.1085	0.0080	0.0249	0.0633	0.0038	0.0125	0.0337
MC_3	FSDT	0.0141	0.0455	0.1011	0.0076	0.0242	0.0624	0.0038	0.0118	0.0332
	FEM	0.0149	0.0471	0.1082	0.0078	0.0248	0.0629	0.0038	0.0125	0.0337
MC_4	FSDT	0.0148	0.0447	0.1006	0.0074	0.0241	0.0613	0.0037	0.0117	0.0329
	FEM	0.0150	0.0467	0.1073	0.0076	0.0245	0.0621	0.0038	0.0124	0.0333
MC_5	FSDT	0.0146	0.0447	0.1006	0.0073	0.0240	0.0610	0.0037	0.0117	0.0329
	FEM	0.0150	0.0466	0.1071	0.0076	0.0244	0.0618	0.0038	0.0124	0.0332
MC_6	FSDT	0.0143	0.0445	0.1003	0.0072	0.0228	0.0607	0.0036	0.0115	0.0323
	FEM	0.0149	0.0461	0.1065	0.0075	0.0233	0.0613	0.0038	0.0121	0.0329
MC_7	FSDT	0.0137	0.0441	0.1001	0.0068	0.0225	0.0602	0.0034	0.0113	0.0321
	FEM	0.0148	0.0459	0.1057	0.0074	0.0230	0.0606	0.0037	0.0119	0.0327
MC_8	FSDT	0.0135	0.0440	0.0998	0.0067	0.0224	0.0602	0.0033	0.0113	0.0323
	FEM	0.0148	0.0458	0.1053	0.0074	0.0229	0.0603	0.0037	0.0121	0.0332

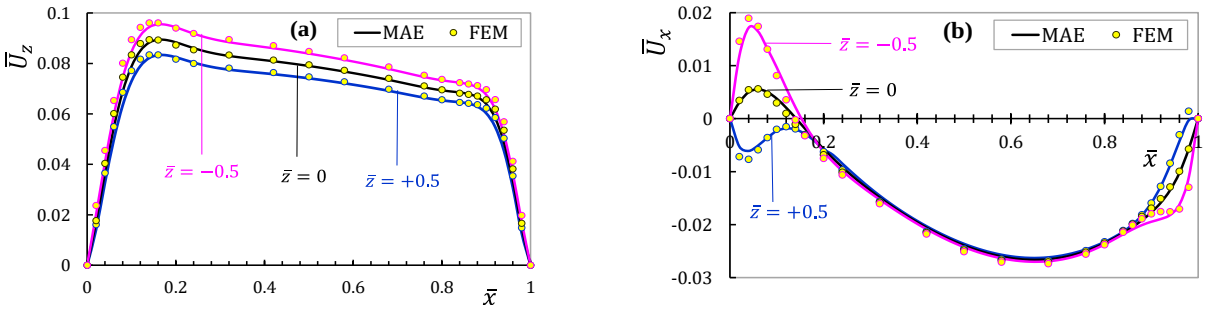

Figure 3. Distribution of displacements along axial direction ($n=2$, $P_i(\bar{x})=P_{i1}$, $h(\bar{x})=h_1$, MC_2).

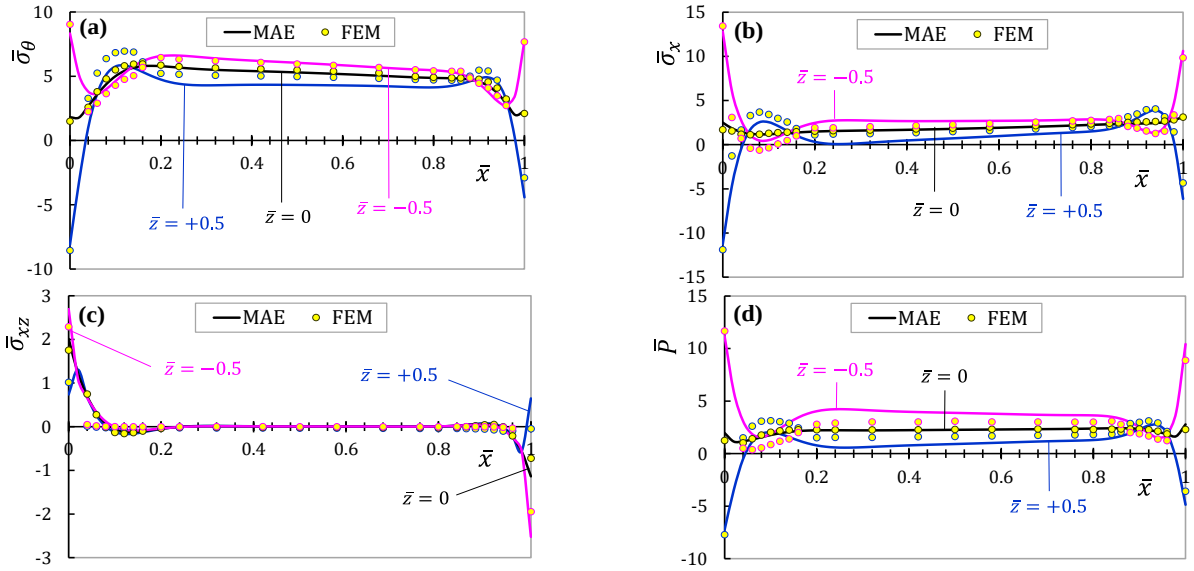

Figure 4. Distribution of (a) circumferential (b) axial (c) shear Cauchy stress and (d) hydrostatic pressure along axial direction ($n=2$, $P_i(\bar{x})=P_{i1}$, $h(\bar{x})=h_1$, MC_2).

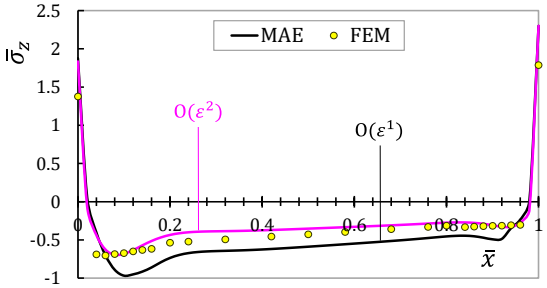

Figure 5. Effect of MAE order on radial Cauchy stress of middle layer.

Fig. 6(a-c) shows the effect of inhomogeneity index on displacements and hydrostatic pressure of internal layer (critical layer). The linear thickness and pressure profile along with MC_1 material constants are considered for shell. Fig. 6(d) shows the variations of dimensionless material constants (normalized to internal layer ones) with power-law distribution along radial direction of a heterogeneous cylinder for integer values of n in the arbitrary range of $-4 \le n \le +4$. The extremum properties of outer layer could be determined through the intersection of vertical line plotted from radius of the point and graph of arbitrary n. Positive values of gradient index increase strength of material under mechanical loading toward outer layer of shell, while the reverse holds true for negative values of n. Hence, variation of inhomogeneity index from negative values to positive ones cause displacements, hydrostatic pressure and consequently stresses of the cylinder to be reduced. Greater values of n intensify improvement or reduction in response of FG shell respect to homogenous one.

Table 6 presents the values of maximum displacements and hydrostatic pressure of layers for different inhomogeneity index and MC_5 material constants. Linear decrease in radial displacement and smooth reduction in axial displacement can be observed from internal layer to the external one for different values of n. Positive values of n cause more uniform hydrostatic pressure distribution of the layers and less maximum values of hydrostatic pressure compared with negative ones. Therefore, It could be concluded that internal layer (in contact with loading) is critical one and positive values of n are more appropriate from the viewpoint of minimal values and uniform distribution of displacements and stresses in heterogeneous cylinder.

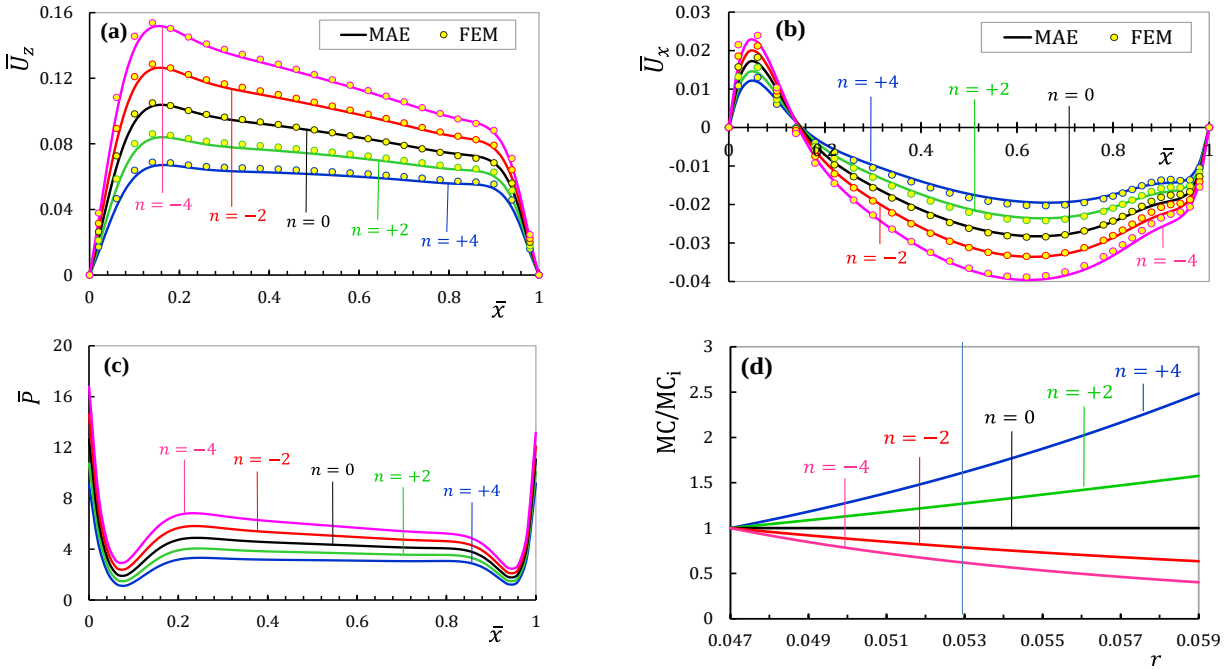

Figure 6. The effect of inhomogeneity index on (a) radial displacement (b) axial displacement (c) hydrostatic pressure (along axial direction of internal layer) and (d) material properties (along radial direction) ($P_i(\bar{x}) = P_{i1}$, $h(\bar{x}) = h_1$, MC_1).

Table 6. Maximum displacements and hydrostatic pressure of layers for different inhomogeneity index ($P_i(\bar{x}) = P_{i1}$, $h(\bar{x}) = h_1$, MC_5).

	$\bar{U}_z$ at $\bar{x}=0.15$			$\bar{U}_x$ at $\bar{x}=0.65$			$\bar{P}$ at $\bar{x}=0$		
	$\bar{z}=-0.5$	$\bar{z}=0$	$\bar{z}=+0.5$	$\bar{z}=-0.5$	$\bar{z}=0$	$\bar{z}=+0.5$	$\bar{z}=-0.5$	$\bar{z}=0$	$\bar{z}=+0.5$
$n=+4$	0.1194	0.1112	0.1029	-0.0398	-0.0394	-0.0389	11.340	2.397	-6.544
$n=+2$	0.1495	0.1391	0.1287	-0.0482	-0.0475	-0.0468	13.408	2.235	-8.937
$n=0$	0.1847	0.1717	0.1588	-0.0578	-0.0568	-0.0559	15.673	1.779	-12.114
$n=-2$	0.2251	0.2092	0.1932	-0.0687	-0.0674	-0.0662	18.127	0.918	-16.291
$n=-4$	0.2707	0.2514	0.2321	-0.0809	-0.0793	-0.0777	20.760	-0.483	-21.726

4.4. Effect of geometry and pressure profiles

The effect of thickness profile on the distribution of displacements under P_{i1} loading are illustrated in Figs. 7 and 8 for heterogeneous cylinder with $n = 2$ and MC_2 materials properties. Considering Fig. 7 prove that changes of concave thickness profile to convex one cause reduction in radial displacement. Low thickness in addition to maximum pressure ascends $\bar{U}_z$ near $\bar{x}=0$ in h_4 thickness profile. It is obviously observed that constant thickness (h_0) have the greatest displacements and stresses under P_{i1}. No considerable variations in axial displacements are observed between non-uniform thickness profiles. Considering Figs. 7 and 8 reveal that pressure profiles increment is more effective on the response of shell respect to thickness profiles

variation; i.e. descending pressure causes more reduction in displacements and stresses respect to the thickness variations.

Table 7 presents the effect of pressure profile on the distribution of displacements and hydrostatic pressure in FG cylinder with the same thickness profile for MC_6. The axial sections are selected based on extremum points of displacements and hydrostatic pressure distribution. The numerical results in different sections of internal layer show that similar thickness and pressure patterns lead in uniform distributions of displacements and hydrostatic pressure along length of the shell. It is observed that linear variation of pressure and thickness counteracts each other effect. This counterbalance descends for nonlinear pressure profiles with similar range of applied pressure. Therefore, radial displacement and hydrostatic pressure ascend form P_{i1},h_1 to P_{i4},h_4 profiles at points far away from boundaries and the effect of pressure profile is dominant. However, the peak values of radial displacement and hydrostatic pressure are nearly close to each other for P_{i1},h_1 to P_{i3},h_3. Considering Table 7, P_{i5},h_5 profiles have the least hydrostatic pressure. In fact, whatever maximum pressure and thickness are considered near clamed boundaries, more counterbalance of thickness and pressure effect occurs. It can be concluded that P_{i5},h_5 and P_{i1},h_1 are appropriate profiles in designing current hyperelastic FG shell.

However, we are not concerned here with possible manufacture processes of FG materials, as well as experimental tests. Authors believe that, when the FG elastomers start to be widely employed in industry or in engineering applications, our formulation is a reliable numerical tool to predict their mechanical behavior (in terms of accuracy). But it is important to note that method presented here will be useful to material scientists in designing new materials, stress analysts, and designers in two states. One can use similar solution procedure to calculate displacements and stresses for FG material models with the given constants functions applied instead of power law distribution. Furthermore, one can control the through-the-thickness distribution of displacements and stresses as objective parameters by tailoring the through-the-thickness variation of the material constants by trial and error to achieve appropriate distribution of FGM constants. In the material tailoring problem, one has found through-the-thickness variation of material constants to achieve a desired variation of stress components, frequency of free vibrations, deformation or an objective function to be optimized [47]. This method is going to be extended in FG elastomers and biological tissues. Bilgili [18] also suggest that the presence of material non-homogeneity in test specimens might be reason for the conflicting experimental results in the technical literature regarding the nature of the rubber-elastic response functions. Hence, he developed comprehensive experimental and theoretical program to characterize the response functions of non-homogeneous rubber components and introduced a design code based on especial (power variation) material model which can explain the essential physics–chemistry behind the intended functionality. This kind of design code yields essential information about the grading which in turn can be used as input into the design of a fabrication process. Thus, our method along with mentioned studies could direct further research toward the design, optimization, and manufacture of graded rubber-like materials.

In recent years, researchers have developed artificial blood vessels made from special elastomer material and the usage of artificial vascular prostheses in vascular graft [48]. Some parts of mentioned prostheses don't have complicated geometries and can be models as regular shells with acceptable tolerances and imperfections. Authors believe that current method could have the potential of helping researchers in the future to analyze and obtain useful information about (a) more realistic hyperelastic material models of blood vessels (artificial or natural, isotropic or anisotropic, homogenous or non-homogeneous); (b) especial variation in internal and /or external profiles of blood vessels resulted from atherosclerotic plaque, aortic aneurysm, aging deformation and so on; (c) maybe future non-homogeneous prosthesis with position dependent functionality.

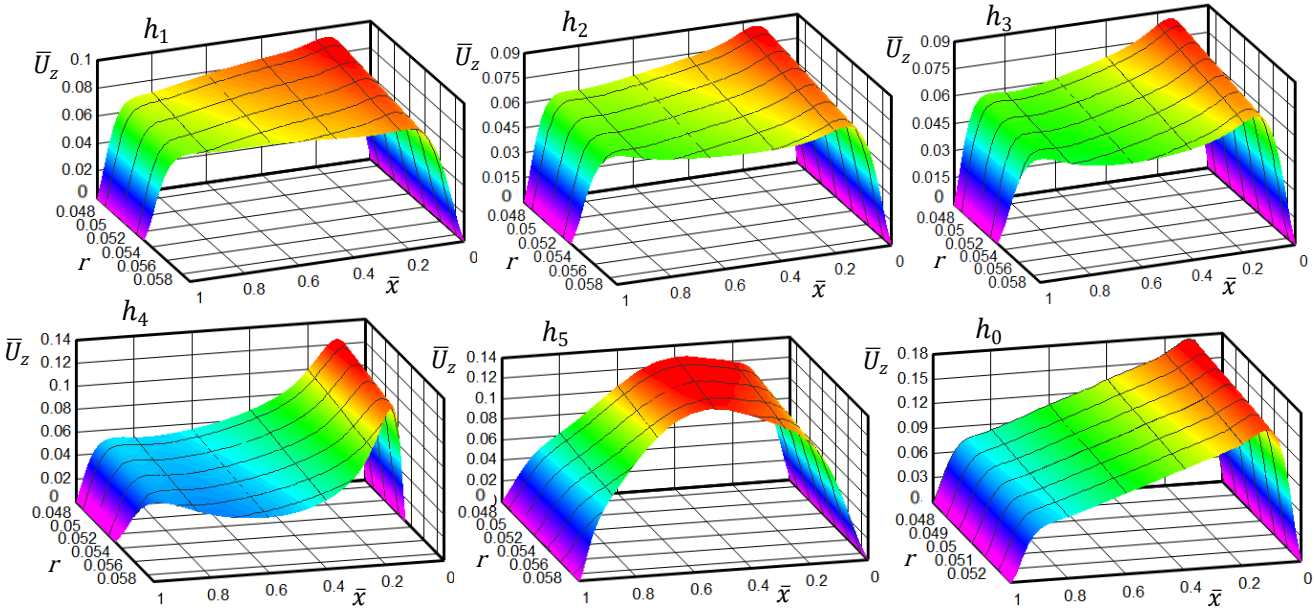

Figure 7. The effect of thickness profile on dimensionless radial displacement ($n=2$, $P_i(\bar{x})=P_{i1}, MC_2$).

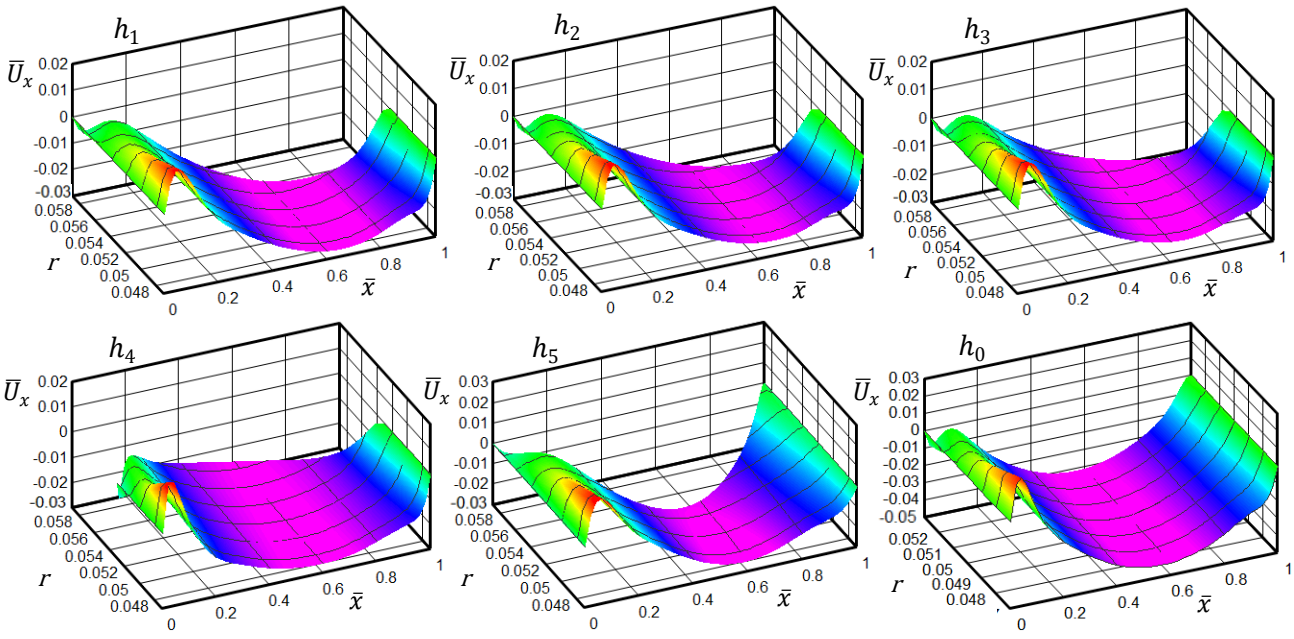

Figure 8. The effect of thickness profile on dimensionless axial displacement ($n=2$, $P_i(\bar{x})=P_{i1}, \mathrm{MC}_2$).

Table 7. Numerical results for similar pressure and thickness profiles at the sections of internal layer ($n=2$, MC_6).

	$\bar{U}_z$			$\bar{U}_x$			$\bar{P}$		
	$\bar{x}=0.15$	$\bar{x}=0.5$	$\bar{x}=0.85$	$\bar{x}=0.05$	$\bar{x}=0.25$	$\bar{x}=0.7$	$\bar{x}=0$	$\bar{x}=0.5$	$\bar{x}=1$
P_{i0}, h_0	0.2483	0.2403	0.2483	0.0408	0.0159	-0.0125	22.595	6.942	22.595
P_{i1}, h_1	0.1820	0.1607	0.1372	0.0266	-0.0205	-0.0601	14.484	5.459	13.016
P_{i2}, h_2	0.1822	0.1695	0.1443	0.0289	-0.0105	-0.0634	14.827	6.096	13.573
P_{i3}, h_3	0.1812	0.1727	0.1505	0.0303	-0.0072	-0.0595	14.813	6.401	14.107
P_{i4}, h_4	0.1609	0.1782	0.1608	0.0422	0.0389	-0.0319	14.762	6.582	14.762
P_{i5}, h_5	0. 1708	0.1196	0.1708	0.0085	-0.0301	0.0297	5.617	4.256	5.618

5. Conclusions

In current research, the heterogonous hyperelastic hollow cylinders with variable thickness under non-uniform internal pressure and clamped boundary conditions have been analyzed by FSDT. Two-term Mooney-Rivlin type material in nearly incompressible condition is considered which is a suitable hyperelastic model for rubbers. The material properties are graded along the radial direction according to a power law function. Match Asymptotic Expansion of the perturbation theory is used for solving the governing equations analytically. The advantages of this method are fast convergence, closed form solution and compatibility with physics of shell. A new ingenious formulation and parameters have been defined during current study to simplify and abbreviate the representation of inner and outer equations components in MAE. In addition, the terms of variable thickness and non-uniform pressure have been presented in separate representation. The results prove the effectiveness of FSDT and MAE combination to derive and solve the governing equations of nonlinear problems such as nearly incompressible hyperelastic shells. The acceptable range of the current analysis for the geometry, loading and materials properties is about $4<\bar{R}<20$ and $P_i/\mu<0.01$ by considering difference percentage of deformations resulted from current analytical solution and FEM less than 10%. An increase in P_i/μ and k or decrease in μ ascend the nonlinearity and difference percentage of numerical and analytical solution. The accuracy of MAE descend for great values of $\bar{R}$ because of intensifying nonlinear behavior of the cylinder while for small $\bar{R}$, the accuracy of shear deformation theory decrease in analyzing thick cylindrical shells. It can be concluded that positive values of gradient index are more appropriate from the viewpoint of less values and more uniform distribution of displacements and stresses in heterogeneous cylinder. It can be concluded that the sequence of effectiveness on the response of shell is pressure profile, thickness variation and finally inhomogeneity index, respectively. Furthermore, changes of concave thickness profile to convex one lead in descending maximum displacement, stresses and hydrostatic pressure. It can be concluded that radial displacement and hydrostatic pressure patterns follow the pattern of the applied pressure function along the length of shell. The behavior of hyperelastic FG vessels under non-uniform pressure distribution show that similar profile of variable thickness and non-uniform applied pressure result in minor displacement and stress quantities and uniform distributions which could be a suitable criterion in designing thickness profile of pressurized vessels. Applying maximum pressure and thickness near the boundaries of shell are suitable profiles for designing hyperelastic FG shells. It is considered that the current methodology could have potential to illustrate the performance of the potentials and their reliability for the prediction of the state of deformation and stress in hyperelastic vessels from rubber pressure vessels to artery blood vessels. Authors believe that current method along with studies mentioned in the literature could direct further researches toward the design, optimization, and manufacture of graded rubber-like materials.

Appendix

The non-homogeneity vectors of $O(\varepsilon^2)$ equations in outer and inner expansions are as follows:

$$\begin{cases}\left\{\mathbf{F}_{O2}^{II}\right\}_1 = Ck_3\left[\left(\overline{II}(2,n-1)+\overline{II}(0,n+1)\right)\bar{\psi}_{O1}^{\ 2}+2\overline{II}(1,n-1)\bar{w}_{O1}\bar{\psi}_{O1}+2\left(\overline{II}(1,n)+\overline{II}(0,n+1)\right)\bar{v}_{O1}\bar{\psi}_{O1}+2\overline{II}(0,n)\bar{v}_{O1}\bar{w}_{O1}+\overline{II}(0,n-1)\bar{w}_{O1}^{\ 2}\right]\\ \qquad +Ck_5\left[\overline{II}(1,n)\bar{\psi}_{O1}^{\ 2}+\overline{II}(0,n)\bar{w}_{O1}\bar{\psi}_{O1}\right]-k\left[\overline{II}(1,n+1)\bar{\varphi}_{O1}'+2\overline{II}(0,n+1)\bar{v}_{O1}^{\ 2}\right]-2\hat{K}_sC_1\overline{II}(0,n+1)\bar{\varphi}_{O1}^{\ 2}, \qquad \left\{\mathbf{F}_{O2}^{II'}\right\}_1=0\end{cases} \tag{A1}$$

$$\begin{cases}\left\{\mathbf{F}_{O2}^{II}\right\}_2 = Ck_2\left[\left(\overline{II}(2,n)+\overline{II}(1,n+1)\right)\bar{\psi}_{O1}'+\overline{II}(1,n)\bar{w}_{O1}'-\left(\overline{II}(1,n)\bar{\psi}_{O1}+\overline{II}(0,n)\bar{w}_{O1}\right)\bar{\varphi}_{O1}+K_s\left(\overline{II}(1,n)\bar{\psi}_{O1}+\overline{II}(0,n)\bar{w}_{O1}\right)\bar{\varphi}_{O1}\right.\\ \qquad \left.+\hat{K}_s\overline{II}(0,n+1)\bar{v}_{O1}\bar{\varphi}_{O1}\right]+2K_sC_1\left(\overline{II}(0,n+1)\bar{w}_{O1}'+\overline{II}(1,n+1)\bar{\psi}_{O1}'\right)-k\,\overline{II}(1,n+1)\bar{v}_{O1}'+\hat{K}_sk\,\overline{II}(0,n+1)\bar{\varphi}_{O1}\bar{\psi}_{O1}\\ \left\{\mathbf{F}_{O2}^{II'}\right\}_2 = Ck_2\left[\overline{II}'(2,n)\bar{\psi}_{O1}+\overline{II}'(1,n)\bar{w}_{O1}+\overline{II}'(1,n+1)\bar{\psi}_{O1}\right]-k\,\overline{II}'(1,n+1)\bar{v}_{O1}\end{cases} \tag{A2}$$

$$\begin{cases}\left\{\mathbf{F}_{O2}^{II}\right\}_3 = -Ck_3\left[\overline{II}(0,n)\left(\bar{v}_{O1}^{\ 2}+\bar{\psi}_{O1}^{\ 2}\right)+2\left(\overline{II}(1,n-1)\bar{\psi}_{O1}+\overline{II}(0,n-1)\bar{w}_{O1}\right)\left(\bar{v}_{O1}+\bar{\psi}_{O1}\right)\right]-2K_sC_1\overline{II}(0,n+1)\bar{\varphi}_{O1}'-Ck_2\overline{II}(1,n)\bar{\varphi}_{O1}'\\ \qquad -Ck_5\overline{II}(0,n)\bar{v}_{O1}\bar{\psi}_{O1}+2k\left[\overline{II}(2,n-2)\bar{\psi}_{O1}^{\ 2}+2\overline{II}(1,n-2)\bar{w}_{O1}\bar{\psi}_{O1}+\overline{II}(0,n-2)\bar{w}_{O1}^{\ 2}\right], \qquad \left\{\mathbf{F}_{O2}^{II'}\right\}_3=-2K_sC_1\overline{II}'(0,n+1)\bar{\varphi}_{O1}\end{cases} \tag{A3}$$

$$\begin{cases}\left\{\mathbf{F}_{O2}^{II}\right\}_4 = -Ck_2\left(\overline{II}(2,n)+\overline{II}(1,n+1)\right)\bar{\varphi}_{O1}'-2K_sC_1\overline{II}(1,n+1)\bar{\varphi}_{O1}'-Ck_3\left[\overline{II}(1,n)\left(3\bar{\psi}_{O1}^{\ 2}+\bar{v}_{O1}^{\ 2}\right)+\overline{II}(2,n-1)\bar{\psi}_{O1}\left(3\bar{\psi}_{O1}+2\bar{v}_{O1}\right)\right.\\ \qquad +\overline{II}(0,n+1)\bar{v}_{O1}\left(2\bar{\psi}_{O1}+\bar{v}_{O1}\right)+\overline{II}(1,n-1)\bar{w}_{O1}\left(4\bar{\psi}_{O1}+2\bar{v}_{O1}\right)+2\overline{II}(0,n)\bar{w}_{O1}\bar{\psi}_{O1}+2\overline{II}(0,n-1)\bar{w}_{O1}^{\ 2}\left.\right]\\ \qquad +2k\left[\overline{II}(1,n-2)\bar{w}_{O1}^{\ 2}+\left(\overline{II}(3,n-2)+\overline{II}(0,n+1)\right)\bar{\psi}_{O1}^{\ 2}+2\overline{II}(2,n-2)\bar{w}_{O1}\bar{\psi}_{O1}\right]\\ \qquad -Ck_5\left[\overline{II}(0,n)\bar{v}_{O1}\bar{w}_{O1}+2\overline{II}(1,n)\bar{v}_{O1}\bar{\psi}_{O1}\right], \qquad \left\{\mathbf{F}_{O2}^{II'}\right\}_4=-2K_sC_1\overline{II}'(1,n+1)\bar{\varphi}_{O1}\end{cases} \tag{A4}$$

$$\left\{\mathbf{F}_{\alpha 2}^{P_\alpha}\right\}_1=\left\{\mathbf{F}_{\alpha 2}^{P_\alpha}\right\}_2=0,\ \left\{\mathbf{F}_{\alpha 2}^{P_\alpha}\right\}_3=-\bar{P}_{i\alpha}\tilde{x}_\alpha\left(\mathrm{D}\bar{R}_\alpha-\frac{\mathrm{D}\bar{h}_\alpha}{2}\right),\ \left\{\mathbf{F}_{\alpha 2}^{P_\alpha}\right\}_4=\bar{P}_{i\alpha}\tilde{x}_\alpha\left(\mathrm{D}\bar{h}_\alpha\bar{R}_\alpha+\bar{h}_\alpha\mathrm{D}\bar{R}_\alpha-\bar{h}_\alpha\mathrm{D}\bar{h}_\alpha\right) \tag{A5}$$

$$\left\{\mathbf{F}_{\alpha 2}^{\mathrm{D}P_\alpha}\right\}_1=\left\{\mathbf{F}_{\alpha 2}^{\mathrm{D}P_\alpha}\right\}_2=0,\quad \left\{\mathbf{F}_{\alpha 2}^{\mathrm{D}P_\alpha}\right\}_3=-\mathrm{D}\bar{P}_{i\alpha}\tilde{x}_\alpha\left(\bar{R}_\alpha-\frac{\bar{h}_\alpha}{2}\right),\quad \left\{\mathbf{F}_{\alpha 2}^{\mathrm{D}P_\alpha}\right\}_4=\frac{\mathrm{D}\bar{P}_{i\alpha}\tilde{x}_\alpha\bar{h}_\alpha}{2}\left(\bar{R}_\alpha-\frac{\bar{h}_\alpha}{2}\right) \tag{A6}$$

$$\begin{aligned}\left\{\mathbf{F}_{\alpha 2}^{II_\alpha}\right\}_1 &= Ck_3\left[2\left(\left(\overline{II}_\alpha(1,n+1)+\overline{II}_\alpha(2,n)\right)\bar{\psi}_{\alpha 1}+\overline{II}_\alpha(1,n)\bar{w}_{\alpha 1}\right)\bar{\varphi}_{\alpha 1}'+\left(\overline{II}_\alpha(0,n+1)+\overline{II}_\alpha(2,n-1)\right)\bar{\psi}_{\alpha 1}^{\ 2}+2\left(\overline{II}_\alpha(1,n)+\overline{II}_\alpha(0,n+1)\right)\bar{v}_{\alpha 1}\bar{\psi}_{\alpha 1}\right.\\ &\quad \left.+2\overline{II}_\alpha(1,n-1)\bar{w}_{\alpha 1}\bar{\psi}_{\alpha 1}+2\overline{II}_\alpha(0,n)\bar{v}_{\alpha 1}\bar{w}_{\alpha 1}+\overline{II}_\alpha(0,n-1)\bar{w}_{\alpha 1}^{\ 2}\right]-2C_1\left[K_s\overline{II}_\alpha(1,n+1)\bar{\varphi}_{\alpha 1}\bar{\psi}_{\alpha 1}'+\overline{II}_\alpha(0,n+1)\left(K_s\bar{\varphi}_{\alpha 1}\bar{w}_{\alpha 1}'+\hat{K}_s\bar{\varphi}_{\alpha 1}^{\ 2}\right)\right]\\ &\quad -k\left[2\overline{II}_\alpha(2,n+1)\left(\bar{\varphi}_{\alpha 1}'\right)^2+4\overline{II}_\alpha(1,n+1)\left(4\bar{v}_{\alpha 1}\bar{\varphi}_{\alpha 1}'-\bar{\varphi}_{\alpha 1}\bar{\psi}_{\alpha 1}'\right)+\overline{II}_\alpha(0,n+1)\left(2\bar{v}_{\alpha 1}^{\ 2}-\bar{\varphi}_{\alpha 1}\bar{w}_{\alpha 1}'\right)\right]+Ck_5\left[\overline{II}_\alpha(1,n)\bar{\psi}_{\alpha 1}^{\ 2}+\overline{II}_\alpha(0,n)\bar{w}_{\alpha 1}\bar{\psi}_{\alpha 1}\right]\end{aligned} \tag{A7}$$

$$\left\{\mathbf{F}_{\alpha 2}^{\mathrm{D}A_\alpha}\right\}_1=\tilde{x}_\alpha Ck_2\left[\left(\mathrm{D}\overline{II}_\alpha(1,n)+\mathrm{D}\overline{II}_\alpha(0,n+1)\right)\bar{\psi}_{\alpha 1}+\mathrm{D}\overline{II}_\alpha(0,n)\bar{w}_{\alpha 1}\right]-\tilde{x}_\alpha k\left(\mathrm{D}\overline{II}_\alpha(1,n+1)\bar{\varphi}_{\alpha 1}'+\mathrm{D}\overline{II}_\alpha(0,n+1)\bar{v}_{\alpha 1}\right) \tag{A8}$$

$$\left\{\mathbf{F}_{\alpha 2}^{\mathrm{D}II_\alpha}\right\}_1=0 \tag{A9}$$

$$\begin{aligned}\left\{\mathbf{F}_{\alpha 2}^{II_\alpha}\right\}_2 &= Ck_2\left[\left(\overline{II}_\alpha(1,n)\bar{\psi}_{\alpha 1}+\overline{II}_\alpha(0,n)\bar{w}_{\alpha 1}+\hat{K}_s\overline{II}_\alpha(0,n+1)\bar{v}_{\alpha 1}\right)\bar{\varphi}_{\alpha 1}+K_s\left(\overline{II}_\alpha(2,n)\bar{\psi}_{\alpha 1}\bar{\psi}_{\alpha 1}'+\overline{II}_\alpha(1,n)\left(\left(\bar{w}_{\alpha 1}\bar{\psi}_{\alpha 1}\right)'+\bar{\psi}_{\alpha 1}\bar{\varphi}_{\alpha 1}\right)\right.\right.\\ &\quad \left.\left.+\overline{II}_\alpha(0,n)\left(\bar{\varphi}_{\alpha 1}+\bar{w}_{\alpha 1}'\right)\bar{w}_{\alpha 1}\right)\right]+K_sCk_1\left[\overline{II}_\alpha(0,n+1)\left(\bar{\psi}_{\alpha 1}+\bar{v}_{\alpha 1}\right)\bar{w}_{\alpha 1}'+\overline{II}_\alpha(1,n+1)\left(\bar{v}_{\alpha 1}+\bar{\psi}_{\alpha 1}\right)\bar{\psi}_{\alpha 1}'\right]\\ &\quad +2Ck_3\left[\overline{II}_\alpha(3,n)\left(\bar{\psi}_{\alpha 1}\bar{\varphi}_{\alpha 1}'\right)'+\overline{II}_\alpha(2,n+1)\bar{\psi}_{\alpha 1}\bar{\varphi}_{\alpha 1}''+\overline{II}_\alpha(1,n+1)\left(\left(\bar{\psi}_{\alpha 1}\bar{v}_{\alpha 1}\right)'+\bar{\psi}_{\alpha 1}\bar{\psi}_{\alpha 1}'\right)+\overline{II}_\alpha(1,n-1)\bar{w}_{\alpha 1}\bar{w}_{\alpha 1}'\right.\\ &\quad \left.+\overline{II}_\alpha(2,n-1)\left(\bar{w}_{\alpha 1}\bar{\psi}_{\alpha 1}\right)'+\overline{II}_\alpha(1,n)\left(\bar{w}_{\alpha 1}\bar{v}_{\alpha 1}\right)'+\overline{II}_\alpha(3,n+1)\bar{\psi}_{\alpha 1}\bar{\psi}_{\alpha 1}'+\overline{II}_\alpha(2,n)\left(\left(\bar{v}_{\alpha 1}\bar{\psi}_{\alpha 1}\right)'+\left(\bar{w}_{\alpha 1}\bar{\varphi}_{\alpha 1}'\right)'\right)\right]\\ &\quad +Ck_4\overline{II}_\alpha(2,n+1)\bar{\psi}_{\alpha 1}'\bar{\varphi}_{\alpha 1}'+Ck_5\left[2\overline{II}_\alpha(2,n)\bar{\psi}_{\alpha 1}\bar{\psi}_{\alpha 1}'+\overline{II}_\alpha(1,n)\left(\bar{w}_{\alpha 1}\bar{\psi}_{\alpha 1}\right)'\right]-2K_sC_1\left[\overline{II}_\alpha(2,n+1)\bar{\psi}_{\alpha 1}''+\overline{II}_\alpha(1,n+1)\bar{w}_{\alpha 1}''\right]\bar{\varphi}_{\alpha 1}\\ &\quad -k\left[\hat{K}_s\overline{II}_\alpha(0,n+1)\bar{\varphi}_{\alpha 1}\bar{\psi}_{\alpha 1}+\overline{II}_\alpha(2,n+1)\left(4\left(\bar{v}_{\alpha 1}\bar{\varphi}_{\alpha 1}'\right)'+K_s\bar{\psi}_{\alpha 1}'\bar{\varphi}_{\alpha 1}'-\bar{\varphi}_{\alpha 1}\bar{\psi}_{\alpha 1}''\right)\right.\\ &\quad \left.+\overline{II}_\alpha(1,n+1)\left(4\bar{v}_{\alpha 1}\bar{v}_{\alpha 1}'-\bar{\varphi}_{\alpha 1}\bar{w}_{\alpha 1}''+\hat{K}_s\left(\bar{w}_{\alpha 1}'+\bar{\varphi}_{\alpha 1}\right)\bar{\varphi}_{\alpha 1}'\right)+4\overline{II}_\alpha(3,n+1)\bar{\varphi}_{\alpha 1}'\bar{\varphi}_{\alpha 1}''\right]\end{aligned} \tag{A10}$$

$$\left\{\mathbf{F}_{\alpha 2}^{\mathrm{DA}_\alpha}\right\}_2 = \tilde{x}_\alpha Ck_2\left[\left(\mathrm{D}\overline{II}_\alpha(2,n)+\mathrm{D}\overline{II}_\alpha(1,n+1)\right)\bar{\psi}_{\alpha 1}'+\mathrm{D}\overline{II}_\alpha(1,n)\bar{w}_{\alpha 1}'\right]-\tilde{x}_\alpha k\left(\mathrm{D}\overline{II}_\alpha(1,n+1)\bar{v}_{\alpha 1}'+\mathrm{D}\overline{II}_\alpha(2,n+1)\bar{\varphi}_{\alpha 1}''\right)$$
$$+2\tilde{x}_\alpha K_s C_1\left[\mathrm{D}\overline{II}_\alpha(1,n+1)\bar{\psi}_{\alpha 1}'+\mathrm{D}\overline{II}_\alpha(0,n+1)\left(\bar{\varphi}_{\alpha 1}+\bar{w}_{\alpha 1}'\right)\right] \tag{A11}$$

$$\left\{\mathbf{F}_{\alpha 2}^{\mathrm{DII}_\alpha}\right\}_2 = Ck_2\left[\left(\mathrm{D}\overline{II}_\alpha(2,n)+\mathrm{D}\overline{II}_\alpha(1,n+1)\right)\bar{\psi}_{\alpha 1}+\mathrm{D}\overline{II}_\alpha(1,n)\bar{w}_{\alpha 1}\right]-k\left(\mathrm{D}\overline{II}_\alpha(1,n+1)\bar{v}_{\alpha 1}+\mathrm{D}\overline{II}_\alpha(2,n+1)\bar{\varphi}_{\alpha 1}'\right) \tag{A12}$$

$$\left\{\mathbf{F}_{\alpha 2}^{II_\alpha}\right\}_3 = Ck_2\Bigg[\overline{II}_\alpha(2,n)\left(\left(1+K_s\right)\bar{\psi}_{\alpha 1}\bar{\psi}_{\alpha 1}''+\hat{K}_s\left(\bar{\psi}_{\alpha 1}'\right)^2\right)-\hat{K}_s\left(\overline{II}_\alpha(1,n+1)\left(\bar{\psi}_{\alpha 1}\bar{\psi}_{\alpha 1}'\right)'+\overline{II}_\alpha(0,n+1)\left(\bar{w}_{\alpha 1}\bar{\psi}_{\alpha 1}\right)'\right)$$
$$+\overline{II}_\alpha(1,n)\left(\bar{w}_{\alpha 1}'\bar{\psi}_{\alpha 1}'+\bar{w}_{\alpha 1}\bar{\psi}_{\alpha 1}''+\bar{\psi}_{\alpha 1}\bar{w}_{\alpha 1}''-\hat{K}_s\bar{\varphi}_{\alpha 1}\bar{\psi}_{\alpha 1}'-K_s\left(2\bar{w}_{\alpha 1}'\bar{\psi}_{\alpha 1}'+\bar{w}_{\alpha 1}\bar{\psi}_{\alpha 1}''+\bar{\psi}_{\alpha 1}\bar{w}_{\alpha 1}''+\bar{\psi}_{\alpha 1}\bar{\varphi}_{\alpha 1}'\right)\right)$$
$$+\overline{II}_\alpha(0,n)\left(2\bar{w}_{\alpha 1}\bar{w}_{\alpha 1}''+\left(\bar{w}_{\alpha 1}'\right)^2-\hat{K}_s\bar{\varphi}_{\alpha 1}\bar{w}_{\alpha 1}'-K_s\left(\left(\bar{w}_{\alpha 1}'\right)^2+\bar{w}_{\alpha 1}\bar{w}_{\alpha 1}''+\bar{w}_{\alpha 1}\bar{\varphi}_{\alpha 1}'\right)\right)\Bigg]-Ck_5\left(\overline{II}_\alpha(0,n)\bar{v}_{\alpha 1}+\overline{II}_\alpha(1,n)\bar{\varphi}_{\alpha 1}'\right)\bar{\psi}_{\alpha 1}$$
$$-Ck_3\Big[2\overline{II}_\alpha(2,n-1)\bar{\psi}_{\alpha 1}\bar{\varphi}_{\alpha 1}'+2\overline{II}_\alpha(0,n-1)\left(\bar{v}_{\alpha 1}+\bar{\psi}_{\alpha 1}\right)\bar{w}_{\alpha 1}+2\overline{II}_\alpha(2,n)\left(\bar{\varphi}_{\alpha 1}'\right)^2+2\overline{II}_\alpha(1,n-1)\left(\bar{w}_{\alpha 1}\bar{\varphi}_{\alpha 1}'+\bar{\psi}_{\alpha 1}^{\,2}+\bar{v}_{\alpha 1}\bar{\psi}_{\alpha 1}\right) \tag{A13}$$
$$+2\overline{II}_\alpha(1,n)\bar{v}_{\alpha 1}\bar{\varphi}_{\alpha 1}'+\overline{II}_\alpha(0,n)\left(\bar{v}_{\alpha 1}^{\,2}+\bar{\psi}_{\alpha 1}^{\,2}\right)\Big]-K_sCk_1\left[\overline{II}_\alpha(1,n+1)\left(\bar{\varphi}_{\alpha 1}\bar{\varphi}_{\alpha 1}'\right)'+\overline{II}_\alpha(0,n+1)\left(\bar{v}_{\alpha 1}\bar{\varphi}_{\alpha 1}+\bar{\varphi}_{\alpha 1}\bar{\psi}_{\alpha 1}\right)'\right]$$
$$+\hat{K}_sk\left[\overline{II}_\alpha(2,n+1)\left(\bar{\varphi}_{\alpha 1}'\bar{\psi}_{\alpha 1}'\right)'+\overline{II}_\alpha(1,n+1)\left(\bar{v}_{\alpha 1}\bar{\psi}_{\alpha 1}'+\bar{\varphi}_{\alpha 1}'\bar{w}_{\alpha 1}'\right)'+\overline{II}_\alpha(0,n+1)\left(\bar{v}_{\alpha 1}\bar{w}_{\alpha 1}'\right)'\right]$$
$$+2k\left[\overline{II}_\alpha(2,n-2)\bar{\psi}_{\alpha 1}^{\,2}+2\overline{II}_\alpha(1,n-2)\bar{w}_{\alpha 1}\bar{\psi}_{\alpha 1}+\overline{II}_\alpha(0,n-2)\bar{w}_{\alpha 1}^{\,2}\right]$$

$$\left\{\mathbf{F}_{\alpha 2}^{\mathrm{DA}_\alpha}\right\}_3 = -\tilde{x}_\alpha Ck_2\left[\mathrm{D}\overline{II}_\alpha(1,n)\bar{\varphi}_{\alpha 1}'+\mathrm{D}\overline{II}_\alpha(0,n)\left(\bar{\psi}_{\alpha 1}+\bar{v}_{\alpha 1}\right)\right]+\tilde{x}_\alpha k\left[\mathrm{D}\overline{II}_\alpha(0,n-1)\bar{w}_{\alpha 1}+\mathrm{D}\overline{II}_\alpha(1,n-1)\bar{\psi}_{\alpha 1}\right]$$
$$-2\tilde{x}_\alpha K_sC_1\left[\mathrm{D}\overline{II}_\alpha(1,n+1)\bar{\psi}_{\alpha 1}''+\mathrm{D}\overline{II}_\alpha(0,n+1)\left(\bar{\varphi}_{\alpha 1}'+\bar{w}_{\alpha 1}''\right)\right] \tag{A14}$$

$$\left\{\mathbf{F}_{\alpha 12}^{\mathrm{DII}_\alpha}\right\}_3 = -2K_sC_1\left[\mathrm{D}\overline{II}_\alpha(1,n+1)\bar{\psi}_{\alpha 1}'+\mathrm{D}\overline{II}_\alpha(0,n+1)\left(\bar{\varphi}_{\alpha 1}+\bar{w}_{\alpha 1}'\right)\right] \tag{A15}$$

$$\left\{\mathbf{F}_{\alpha 2}^{II_\alpha}\right\}_4 = -Ck_2\Bigg[\overline{II}_\alpha(0,n+1)\bar{\varphi}_{\alpha 1}\bar{w}_{\alpha 1}'+\hat{K}_s\left(\overline{II}_\alpha(1,n+1)\bar{w}_{\alpha 1}''+\overline{II}_\alpha(2,n+1)\bar{\psi}_{\alpha 1}''\right)\bar{\psi}_{\alpha 1}+\overline{II}_\alpha(3,n)\left(2K_s\bar{\psi}_{\alpha 1}\bar{\psi}_{\alpha 1}''-\hat{K}_s\left(\bar{\psi}_{\alpha 1}'\right)^2-\bar{\psi}_{\alpha 1}\bar{\psi}_{\alpha 1}''\right)$$
$$+\overline{II}_\alpha(2,n)\left(K_s\left(+\bar{\psi}_{\alpha 1}\bar{\varphi}_{\alpha 1}'\right)+\hat{K}_s\left(\bar{\varphi}_{\alpha 1}\bar{w}_{\alpha 1}'-\left(\bar{w}_{\alpha 1}\bar{\psi}_{\alpha 1}'\right)'-\bar{\psi}_{\alpha 1}\bar{w}_{\alpha 1}''\right)\right)+\overline{II}_\alpha(1,n)\left(K_s\bar{w}_{\alpha 1}\bar{\varphi}_{\alpha 1}'+\hat{K}_s\left(\bar{\varphi}_{\alpha 1}\bar{w}_{\alpha 1}'-\left(\bar{w}_{\alpha 1}'\right)^2-\bar{w}_{\alpha 1}\bar{w}_{\alpha 1}''\right)\right)\Bigg]$$
$$+2C_1\overline{II}_\alpha(0,n+1)\left(\hat{K}_s\left(\bar{w}_{\alpha 1}'\right)^2+K_s\bar{\varphi}_{\alpha 1}\bar{w}_{\alpha 1}'\right)-Ck_3\Big[\overline{II}_\alpha(3,n)\left(\bar{\varphi}_{\alpha 1}'\right)^2+\overline{II}_\alpha(0,n-1)\bar{w}_{\alpha 1}^{\,2}+2\overline{II}_\alpha(1,n+1)\left(\bar{v}_{\alpha 1}+\bar{\psi}_{\alpha 1}\right)\bar{\varphi}_{\alpha 1}'$$
$$+2\left(\overline{II}_\alpha(2,n-1)+\overline{II}_\alpha(0,n+1)\right)\bar{v}_{\alpha 1}\bar{\psi}_{\alpha 1}+2\left(2\overline{II}_\alpha(1,n-1)+\overline{II}_\alpha(0,n)\right)\bar{w}_{\alpha 1}\bar{\psi}_{\alpha 1}+\left(\overline{II}_\alpha(0,n+1)+\overline{II}_\alpha(1,n)\right)\bar{v}_{\alpha 1}^{\,2}+2\overline{II}_\alpha(2,n)\bar{v}_{\alpha 1}\bar{\varphi}_{\alpha 1}'$$
$$+3\left(\overline{II}_\alpha(1,n)+\overline{II}_\alpha(2,n-1)\right)\bar{\psi}_{\alpha 1}^{\,2}+2\overline{II}_\alpha(1,n-1)\bar{v}_{\alpha 1}\bar{w}_{\alpha 1}+2\overline{II}_\alpha(2,n-1)\bar{w}_{\alpha 1}\bar{\varphi}_{\alpha 1}'+2\overline{II}_\alpha(3,n-1)\bar{\psi}_{\alpha 1}\bar{\varphi}_{\alpha 1}'+\overline{II}_\alpha(2,n+1)\left(\bar{\varphi}_{\alpha 1}'\right)^2\Big] \tag{A16}$$
$$-Ck_1\left[\overline{II}_\alpha(2,n+1)\left(\hat{K}_s\left(\bar{\psi}_{\alpha 1}'\right)^2+K_s\left(\bar{\varphi}_{\alpha 1}\bar{\varphi}_{\alpha 1}'\right)'\right)+K_s\,\overline{II}_\alpha(1,n+1)\left(\left(\bar{\varphi}_{\alpha 1}\bar{v}_{\alpha 1}\right)'+\bar{\psi}_{\alpha 1}\bar{\varphi}_{\alpha 1}'\right)\right]$$
$$-Ck_5\left[2\overline{II}_\alpha(2,n)\bar{\psi}_{\alpha 1}\bar{\varphi}_{\alpha 1}'+2\overline{II}_\alpha(1,n)\left(\bar{v}_{\alpha 1}\bar{\psi}_{\alpha 1}+\bar{w}_{\alpha 1}\bar{\varphi}_{\alpha 1}'\right)+\overline{II}_\alpha(0,n)\bar{v}_{\alpha 1}\bar{w}_{\alpha 1}\right]$$
$$+\hat{K}_sk\left[\overline{II}_\alpha(3,n+1)\left(\bar{\varphi}_{\alpha 1}'\bar{\psi}_{\alpha 1}'\right)'+\overline{II}_\alpha(2,n+1)\left(\left(\bar{\varphi}_{\alpha 1}'\bar{w}_{\alpha 1}'\right)'+\left(\bar{v}_{\alpha 1}\bar{\psi}_{\alpha 1}'\right)'\right)+\overline{II}_\alpha(1,n+1)\left(\left(\bar{v}_{\alpha 1}\bar{w}_{\alpha 1}'\right)'+\left(\bar{w}_{\alpha 1}'+\bar{\varphi}_{\alpha 1}\right)\bar{\psi}_{\alpha 1}'\right)\right]$$
$$+2k\left[\overline{II}_\alpha(1,n-2)\bar{w}_{\alpha 1}^{\,2}+\left(\overline{II}_\alpha(3,n-2)+\overline{II}_\alpha(0,n+1)\right)\bar{\psi}_{\alpha 1}^{\,2}+2\overline{II}_\alpha(2,n-2)\bar{w}_{\alpha 1}\bar{\psi}_{\alpha 1}\right]$$

$$\left\{\mathbf{F}_{\alpha 2}^{\mathrm{DA}_\alpha}\right\}_4 = -\tilde{x}_\alpha Ck_2\left[\mathrm{D}\overline{II}_\alpha(0,n+1)\left(\bar{v}_{\alpha 1}\right)+\mathrm{D}\overline{II}_\alpha(1,n)\left(2\bar{\psi}_{\alpha 1}+\bar{v}_{\alpha 1}\right)+\mathrm{D}\overline{II}_\alpha(0,n)\left(\bar{w}_{\alpha 1}\right)+\left(\mathrm{D}\overline{II}_\alpha(2,n)+\mathrm{D}\overline{II}_\alpha(1,n+1)\right)\bar{\varphi}_{\alpha 1}'\right]$$
$$-2\tilde{x}_\alpha K_sC_1\left[\mathrm{D}\overline{II}_\alpha(2,n+1)\bar{\psi}_{\alpha 1}''+\mathrm{D}\overline{II}_\alpha(1,n+1)\left(\bar{\varphi}_{\alpha 1}'+\bar{w}_{\alpha 1}''\right)\right]+\tilde{x}_\alpha k\left[\left(\mathrm{D}\overline{II}_\alpha(2,n-1)+\mathrm{D}\overline{II}_\alpha(0,n+1)\right)\bar{\psi}_{\alpha 1}+\mathrm{D}\overline{II}_\alpha(1,n-1)\bar{w}_{\alpha 1}\right] \tag{A17}$$

$$\left\{\mathbf{F}_{\alpha 2}^{\mathrm{DII}_\alpha}\right\}_4 = -2K_sC_1\left[\mathrm{D}\overline{II}_\alpha(2,n+1)\bar{\psi}_{\alpha 1}'+\mathrm{D}\overline{II}_\alpha(1,n+1)\left(\bar{\varphi}_{\alpha 1}+\bar{w}_{\alpha 1}'\right)\right] \tag{A18}$$

References

[1] M. C. Boyce, E. M. Arruda, Constitutive Models of Rubber Elasticity: A Review, *Rubber Chemistry and Technology*, Vol. 73, No. 3, pp. 504-523, 2000.

[2] T. Sussman, K.-J. Bathe, A finite element formulation for nonlinear incompressible elastic and inelastic analysis, *Computers & Structures*, Vol. 26, No. 1-2, pp. 357-409, 1987.

[3] S. Doll, K. Schweizerhof, On the Development of Volumetric Strain Energy Functions, *Journal of Applied Mechanics*, Vol. 67, No. 1, 2000.

[4] O. Lopez-Pamies, A new -based hyperelastic model for rubber elastic materials, *Comptes Rendus Mécanique*, Vol. 338, No. 1, pp. 3-11, 2010.

[5] I. Bijelonja, I. Demirdžić, S. Muzaferija, A finite volume method for large strain analysis of incompressible hyperelastic materials, *International Journal for Numerical Methods in Engineering*, Vol. 64, No. 12, pp. 1594-1609, 2005.

[6] Y. Zhu, X. Y. Luo, R. W. Ogden, Nonlinear axisymmetric deformations of an elastic tube under external pressure, *European Journal of Mechanics - A/Solids*, Vol. 29, No. 2, pp. 216-229, 2010.

[7] M. Tanveer, J. W. Zu, Non-linear vibration of hyperelastic axisymmetric solids by a mixed p-type method, *International Journal of Non-Linear Mechanics*, Vol. 47, No. 4, pp. 30-41, 2012.

[8] G. Montella, A. Calabrese, G. Serino, Mechanical characterization of a Tire Derived Material: Experiments, hyperelastic modeling and numerical validation, *Construction and Building Materials*, Vol. 66, pp. 336-347, 2014.

[9] J. Kiendl, M.-C. Hsu, M. C. H. Wu, A. Reali, Isogeometric Kirchhoff–Love shell formulations for general hyperelastic materials, *Computer Methods in Applied Mechanics and Engineering*, Vol. 291, pp. 280-303, 2015.

[10] D. Azar, D. Ohadi, A. Rachev, J. F. Eberth, M. J. Uline, T. Shazly, Mechanical and geometrical determinants of wall stress in abdominal aortic aneurysms: A computational study, *PLoS One*, Vol. 13, No. 2, pp. e0192032, 2018.

[11] J. Vossoughi, A. Tozeren, Determination of an effective shear modulus of aorta, *Russian Journal of Biomechanics*, Vol. 1-2, pp. 20-36, 1998.

[12] L. A. Mihai, A. Goriely, How to characterize a nonlinear elastic material? A review on nonlinear constitutive parameters in isotropic finite elasticity, *Proceedings. Mathematical, physical, and engineering sciences Royal Society*, Vol. 473, No. 2207, pp. 20170607, 2017.

[13] C. M. Scotti, A. D. Shkolnik, S. C. Muluk, E. A. Finol, Fluid-structure interaction in abdominal aortic aneurysms: effects of asymmetry and wall thickness, *BioMedical Engineering OnLine*, Vol. 4, pp. 1-22, 2005.

[14] C. Lally, F. Dolan, P. J. Prendergast, Cardiovascular stent design and vessel stresses: a finite element analysis, *Journal of Biomechanics*, Vol. 38, No. 8, pp. 1574-81, 2005.

[15] G. Chagnon, M. Rebouah, D. Favier, Hyperelastic Energy Densities for Soft Biological Tissues: A Review, *Journal of Elasticity*, Vol. 120, No. 2, pp. 129-160, 2014.

[16] Y. Ikeda, Y. Kasai, S. Murakami, S. Kohjiya, Preparation and Mechanical Properties of Graded Styrene-Butadiene Rubber Vulcanizates, *Journal of the Japan Institute of Metals*, Vol. 62, No. 11, pp. 1013-1017, 1998.

[17] E. Bilgili, Controlling the stress–strain inhomogeneities in axially sheared and radially heated hollow rubber tubes via functional grading, *Mechanics Research Communications*, Vol. 30, No. 3, pp. 257-266, 2003.

[18] E. Bilgili, Modelling mechanical behaviour of continuously graded vulcanised rubbers, *Plastics, Rubber and Composites*, Vol. 33, No. 4, pp. 163-169, 2013.

[19] O. Lopez-Pamies, P. Ponte Castañeda, On the overall behavior, microstructure evolution, and macroscopic stability in reinforced rubbers at large deformations: I—Theory, *Journal of the Mechanics and Physics of Solids*, Vol. 54, No. 4, pp. 807-830, 2006.

[20] R. C. Batra, A. Bahrami, Inflation and eversion of functionally graded non-linear elastic incompressible circular cylinders, *International Journal of Non-Linear Mechanics*, Vol. 44, No. 3, pp. 311-323, 2009.

[21] Y. Anani, G. H. Rahimi, Stress analysis of thick pressure vessel composed of functionally graded incompressible hyperelastic materials, *International Journal of Mechanical Sciences*, Vol. 104, pp. 1-7, 2015.

[22] Y. Anani, G. H. Rahimi, Stress analysis of rotating cylindrical shell composed of functionally graded incompressible hyperelastic materials, *International Journal of Mechanical Sciences*, Vol. 108-109, pp. 122-128, 2016.

[23] M. H. Ghadiri Rad, F. Shahabian, S. M. Hosseini, Geometrically nonlinear elastodynamic analysis of hyper-elastic neo-Hooken FG cylinder subjected to shock loading using MLPG method, *Engineering Analysis with Boundary Elements*, Vol. 50, pp. 83-96, 2015.

[24] H. R. Eipakchi, Third-order shear deformation theory for stress analysis of a thick conical shell under pressure, *Journal of Mechanics of Materials and Structures*, Vol. 5, No. 1, pp. 1-17, 2010.

[25] H. Gharooni, M. Ghannad, M. Z. Nejad, Thermo-Elastic Analysis of Clamped-Clamped Thick FGM Cylinders by Using Third-Order Shear Deformation Theory, *Latin American Journal of Solids and Structures*, Vol. 13, No. 4, pp. 750-774, 2016.

[26] M. Ghannad, G. H. Rahimi, M. Z. Nejad, Elastic analysis of pressurized thick cylindrical shells with variable thickness made of functionally graded materials, *Composites Part B: Engineering*, Vol. 45, No. 1, pp. 388-396, 2013.

[27] M. Jabbari, M. Z. Nejad, M. Ghannad, Thermo-elastic analysis of axially functionally graded rotating thick truncated conical shells with varying thickness, *Composites Part B: Engineering*, Vol. 96, pp. 20-34, 2016.

[28] M. Z. Nejad, M. Jabbari, M. Ghannad, Elastic analysis of axially functionally graded rotating thick cylinder with variable thickness under non-uniform arbitrarily pressure loading, *International Journal of Engineering Science*, Vol. 89, pp. 86-99, 2015.

[29] Z. Mazarei, M. Z. Nejad, A. Hadi, Thermo-Elasto-Plastic Analysis of Thick-Walled Spherical Pressure Vessels Made of Functionally Graded Materials, *International Journal of Applied Mechanics*, Vol. 08, No. 04, 2016.

[30] M. Z. Nejad, N. Alamzadeh, A. Hadi, Thermoelastoplastic analysis of FGM rotating thick cylindrical pressure vessels in linear elastic-fully plastic condition, *Composites Part B: Engineering*, Vol. 154, pp. 410-422, 2018.

[31] M. Hosseini, M. Shishesaz, A. Hadi, Thermoelastic analysis of rotating functionally graded micro/nanodisks of variable thickness, *Thin-Walled Structures*, Vol. 134, pp. 508-523, 2019.

[32] M. Z. Nejad, A. Hadi, Non-local analysis of free vibration of bi-directional functionally graded Euler–Bernoulli nano-beams, *International Journal of Engineering Science*, Vol. 105, pp. 1-11, 2016.

[33] M. Z. Nejad, A. Hadi, A. Rastgoo, Buckling analysis of arbitrary two-directional functionally graded Euler–Bernoulli nano-beams based on nonlocal elasticity theory, *International Journal of Engineering Science*, Vol. 103, pp. 1-10, 2016.

[34] M. Z. Nejad, A. Hadi, A. Omidvari, A. Rastgoo, Bending analysis of bi-directional functionally graded Euler-Bernoulli nano-beams using integral form of Eringen\'s non-local elasticity theory, *Structural Engineering and Mechanics*, Vol. 67, No. 4, pp. 417-425, 2018.

[35] H. Ghaemi, K. Behdinan, A. Spence, On the development of compressible pseudo-strain energy density function for elastomers, *Journal of Materials Processing Technology*, Vol. 178, No. 1-3, pp. 307-316, 2006.

[36] C. A. C. SILVA, M. L. BITTENCOURT, Structural shape optimization of 3D nearly-incompressible hyperelasticity problems, *Latin American Journal of Solids and Structures*, Vol. 5, No. 2, pp. 129-156, 2008.

[37] G. A. Holzapfel, 2000, *Nonlinear Solid Mechanics, a Continuum Approach for Engineering*, Wiley, New York

[38] Y. Başar, D. Weichert, 2000, *Nonlinear Continuum Mechanics of Solids*, Springer, Berlin

[39] J. H. Kim, S. Avril, A. Duprey, J. P. Favre, Experimental characterization of rupture in human aortic aneurysms using a full-field measurement technique, *Biomechanics and Modeling in Mechanobiology*, Vol. 11, No. 6, pp. 841-853, 2012.

[40] I. Doghri, 2000, *Mechanics of Deformable Solids*, Springer, Berlin

[41] A. H. Nayfeh, 1993, *Introduction to Perturbation Techniques*, Wiley, New York

[42] V. Dias, C. Odenbreit, O. Hechler, F. Scholzen, T. Ben Zineb, Development of a constitutive hyperelastic material law for numerical simulations of adhesive steel–glass connections using structural silicone, *International Journal of Adhesion and Adhesives*, Vol. 48, pp. 194-209, 2014.

[43] A. P. S. Selvadurai, M. Shi, Fluid pressure loading of a hyperelastic membrane, *International Journal of Non-Linear Mechanics*, Vol. 47, No. 2, pp. 228-239, 2012.

[44] G. A. Holzapfel, T. C. Gasser, Computational stress-deformation analysis of arterial walls including high-pressure response, *International Journal of Cardiology*, Vol. 116, No. 1, pp. 78-85, 2007.

[45] M. Abdessamad, M. Hasnaoui, M. Agouzoul, Analytical Modeling of a Descending Aorta Containing Human Blood Flow, *Defect and Diffusion Forum*, Vol. 384, pp. 117-129, 2018.

[46] J. D. Humphrey, S. L. O'Rourke, 2015, *An Introduction to Biomechanics: Solids and Fluids, Analysis and Design*, Springer, New York, 2nded.

[47] R. C. Batra, Material tailoring and universal relations for axisymmetric deformations of functionally graded rubberlike cylinders and spheres, *Mathematics and Mechanics of Solids*, Vol. 16, No. 7, pp. 729-738, 2011.

[48] M. J. Łos, S. Panigrahi, K. Sielatycka, C. Grillon, *Successful Biomaterial-Based Artificial Organ—Updates on Artificial Blood Vessels*, in: M. J. Łos, A. Hudecki, E. Wiecheć, *Stem Cells and Biomaterials for Regenerative Medicine*, Eds., pp. 203-222, United States: Academic Press, 2019.